© 2009

Erhan Ilkmen

INTRACAVITY OPTOGALVANIC SPECTROSCOPY FOR

RADIOCARBON ANALYSIS WITH ATTOMOLE SENSITIVITY

By Erhan Ilkmen

A dissertation submitted to the

Graduate School – Newark

Rutgers, The State University of New Jersey

in partial fulfillment of the requirements

for the degree of

Doctor of Philosophy

Graduate Program in Applied Physics

Written under the direction of

Professor Daniel E. Murnick

and approved by

_____

_____

_____

_____

Newark, New Jersey

October 2009

ABSTRACT

Intracavity Optogalvanic Spectroscopy - Radiocarbon Analysis With Attomole

Sensitivity

By Erhan Ilkmen

Thesis Director: Professor Daniel E. Murnick

Carbon-14 (radiocarbon) is a naturally occurring radioactive isotope of carbon, having an extremely low natural abundance in living organisms (^{14}C/C ~ 10^{-12}) and a long half life of ~ 5730 years. These properties make it an ideal organic tracer for various applications in biological, pharmaceutical and environmental sciences as well as carbon dating. Today, the state of the art radiocarbon quantitation technique is Accelerator Mass Spectrometry (AMS) which is based on ion counting using a several megavolt tandem electrostatic accelerator as a mass spectrometer. Although AMS sets the standard for high sensitivity detection, its size, cost and complexity as an analysis system, limits its wide and routine use especially in laboratory or field applications. In this thesis, a new ultra-sensitive laser based analytical technique that can quantify attomoles of ^{14}C in submicrogram samples is demonstrated. The new system exhibits similar or better measurement capabilities as AMS, in sensitivity (^{14}C/C $\leq 10^{-15}$), precision ($\leq$3%) and accuracy ($\leq$5%). Additional advantages include non destructive analysis capability, small size, being a table top instrument, high sample throughput capability via flow processing and the potential to be coupled to GC/LC instrumentation.

The developed Intracavity Optogalvanic Spectroscopy (ICOGS) system is based on measuring changes in electrical properties of a weakly ionized glow discharge placed inside the cavity of a periodically modulated high power (50 W) ^{14}CO$_2$ laser. This new

configuration enabled improvement of the signal detection sensitivity by about six orders of magnitude compared to the conventional external cell optogalvanic spectroscopy method. The signal enhancement mechanism is similar to, but with key differences from the well studied optical detection method Intracavity Absorption Spectroscopy (ICAS). Measurement capability of this new system is demonstrated with calibration curves relative to AMS measurements with a dynamic range of more than five orders of magnitude. The systems studied exhibited saturation effects with laser power and measurement time and also non-linearities in response with samples having enrichments greater than 12 Modern. (1 Modern = 1.10^{-12} $^{14}C/^{12}C$ ratio.) However, standard operating procedures were developed for accurately measuring unknown samples. For a more thorough quantitative understanding of the enhancement mechanism, a physical rate equations model has been outlined.

ACKNOWLEDGEMENTS

I would like to express my gratitude to those who helped me with my graduate career as well those who showed greatest support and made sacrifices throughout my life. First, I would like to thank my advisor Prof. Daniel Murnick for his guidance and support throughout my years at Rutgers. I would like to acknowledge Dr. Ozgur Dogru, Dr. Karina Schafer and Mark DeGuzman who have contributed in various ways throughout this project. I also appreciate the contributions of my thesis committee members Prof. Martin Schaden, Prof. Zhen Wu, Prof. Gene Hall and Prof. Robert Barat with their insightful comments and questions.

I would like to extend my deepest gratitude to my family for their emotional and financial support to pursue my education in the United States. Finally, I am deeply grateful to my wife Yasemin who was there beside me with her love and confidence which made this thesis possible.

TABLE OF CONTENTS

LIST OF FIGURES

Chapter 1 : Introduction

1.1 Properties of ^{14}C

^{14}C is a naturally occurring radioisotope of carbon. Compared to other more abundant isotopes, namely ^{12}C (98.9%) and ^{13}C (1.1%), ^{14}C constitutes only 10^{-10}% of all carbon in the atmosphere. ^{14}C decays into ^{14}N by beta emission with a maximum radiation energy of 0.156 MeV and has a half life of 5730 ± 40 years. The specific activity of ^{14}C in living organisms is about 6.11 picoCuries per gram of carbon and the decay rate is 13.6 disintegrations per minute (dpm) per gram carbon. In nature, it is mainly found in the form of ^{14}CO$_2$ and the total ^{14}C content of an average human that weighs 70 kg is about 77 nanoCuries. Carbon-14 is widely used as a tracer molecule in biochemistry and atmospheric sciences.

1.2 Background

The existence of ^{14}C was first hypothesized by Franz N. Kurie in 1934 as he studied neutron disintegration of nitrogen at the Radiation Lab in University of California in Berkeley. [1] Later in 1939, during their studies with high altitude balloons carrying sensitive neutron detectors, Serge Korff and his colleagues discovered that high energy cosmic rays incident on earth react with gasses in the upper atmosphere to produce secondary, or slow, neutrons. They observed higher neutron count rates at higher altitudes and concluded that the reason for decrease in the number of neutrons that reach to the earth is because they react with nitrogen-14 to eliminate a proton and turn it into radioactive Carbon 14. [2,3]

The first laboratory production of ^{14}C was carried out by Martin Kamen and Sam Ruben in 1940, at the Radiation Lab in UC Berkeley. Their research included radioactive tracers to study the plants' metabolism pathways. By bombarding graphite with deuterons with energies of 3-4 MeV in a cyclotron, they successfully produced long lived radioactivity. They also found that irradiation of nitrogen with slow neutrons yield higher specific activities and this proved to be a more practical method for ^{14}C production. Another important result was their estimation of the half life of ^{14}C. The radioactive half life of ^{14}C is now known to be 5730 years and back then they estimated to be between 10^3 to 10^5 years [4].

The discovery of ^{14}C in the nature and improved understanding of its production mechanism, led to the development of radiocarbon dating technique. Assuming that the cosmic radiation is relatively constant over several tens of thousands of years, the radiocarbon concentration in the atmosphere reaches an equilibrium with respect to more abundant isotopes of Carbon (^{14}C/C ~ 1.2 x 10^{-12}). In addition, this ratio must be constant in all living organisms because of the carbon exchange cycle between the atmosphere and biosphere. However, when a living organism dies, it ceases to exchange carbon with its surroundings and the ^{14}C gets depleted via radioactive decay. In 1946, Willard Libby showed that it's possible to determine the age of an organism by comparing its recent isotopic ratio with the known atmospheric abundance ratio. [5,6] Libby won the 1960 Nobel Prize in Chemistry for this discovery.

In 1955, Hans Suess demonstrated that the carbon dating standards need to be corrected because the isotopic ratio has been altered as a result of increased fossil fuel burning starting with the industrial revolution [7]. The fossil fuels contain no ^{14}C since they are

the product of dead plants and animals and have formed over hundreds of millions of years. Suess effect is becoming more profound as the higher demand for energy leads to more fossil fuel combustion. According to Intergovernmental Panel on Climate Change's Fourth Assessment Report, amount of carbon dioxide in the atmosphere has increased from 3.2 billion tonnes per year to 4.1 billion tonnes per year solely from human causes [8] while the ^{14}C production via cosmic radiation has stayed stable around 6 kg per year. Accurate isotopic abundance measurements provide critical data that can be analyzed and interpreted to determine the sources and sinks for anthropogenic CO_2 emissions that may lead to global warming.

Another significant effect on the contemporary amount of atmospheric radiocarbon was the atomic bomb tests between late 1950's and early 1980's. The peak period of weapons test were in 1960 and 1961 and it is estimated that 9.6 MCi of radiocarbon were introduced to the upper atmosphere during these tests which brought the total radiocarbon budget to 13.4 MCi in the atmosphere [9].

This three fold increase in the radiocarbon budget in the atmosphere has become a major part of the environmental research field in which the scientists use ^{14}C as a tracer molecule to study the dynamics of carbon exchange between the atmosphere, the biosphere and the oceans. [10-12]

1.3 ^{14}C as a Biomedical Tracer

In addition to atmospheric sciences, ^{14}C has wide range of uses in biomedical and pharmaceutical research. An important application involves radiocarbon tags which are used in determining the absorption and metabolism pathways of drugs at the R&D phase. A possible drug candidate is evaluated for its kinetic and dynamic properties via

absorption, distribution, metabolism and excretion (ADME) studies. [13]. However, administration of radioactive tracers directly to humans may have damaging health effects. Therefore, United States Nuclear Regulatory Commission (NRC) has set the Annual Limit of Intake (ALI) for ^{14}C at 2 mCi either via ingestion or inhalation. Recent developments in ^{14}C quantification techniques such as Accelerator Mass Spectrometry and ICOGS enable microdosing studies which includes administration of sub-therapeutic doses of drug candidates. [17-19]

1.4 Radiocarbon Detection and Analysis Techniques

Scintillation counters and Accelerator Mass Spectrometers have been the most widely used analytical methods for detection of radiocarbon and determining the isotopic ratio of a given sample. Earliest radiation detectors were based on counting the decay events from ^{14}C. As the beta emissions pass through a Geiger counter, they ionize the gas inside the detector which can be detected as an electrical pulse. Although this is a highly efficient radioactivity detection method, due to long half life and low specific activity of radiocarbon (13.6 dpm per gram carbon), rapid analysis, especially for biomedical applications, requires administration of high radioactivity which introduces several safety issues.

Highest sensitivity via decay counting is achieved by the Liquid Scintillation Counters (LSC). In this technique, the radioactive sample is placed inside a liquid "cocktail" that contain fluorescent molecules which emit photon as they react with beta emission. Subsequently, the photo multiplier tubes of the LSC register these photons as electrical signals proportional to the amount of radioactivity of the sample. These high precision radioactivity detectors are limited in sensitivity and several engineering challenges exist

to tackle the effects of background radiation and the quenching phenomenon which limit the efficiency. Especially for studies with samples with doses that are relevant to human physiology (e.g. micrograms of samples that should contain picomoles of ^{14}C), LSC's are not the preferred instruments for routine ^{14}C analysis. [14-15].

State of the art analytical method for isotopic analysis of radiocarbon and other long lived radioisotopes is the Accelerator Mass Spectrometry. Capable of analyzing isotopic ratios between 10^{-15} to 10^{-8} in mg samples, which imply attomole sensitivity levels, AMS technique provides as much as 10^9 times higher sensitivity than scintillation counters.

This method was initially developed for more efficient radiocarbon dating applications, allowing analysis of much smaller samples, since LSC requires count rates greater than 10 dpm which implies the requirement of $\sim 10^{10}$ or more atoms of ^{14}C. [16] AMS, on the other hand, does not rely on decay events and counts ions via mass spectrometry. This technique uses a several megavolt tandem electrostatic accelerator as a mass spectrometers (Figure 1.1). Negative ions are formed via a cesium sputter from samples that have been reduced to solid graphite and introduced into a low energy (20-100 keV/ion) spectrometer. This is an extremely important step to distinguish the ^{14}N isobar from the ^{14}C samples. Since the ground state triplet of negative ^{14}N ion is unstable (lifetime $\sim 5 \times 10^{-14}$ sec), this step helps eliminate equal mass atoms from reaching detector that would otherwise lead to inaccurate measurements. From here the ion beam is steered into the 5-10 MV accelerator in which the negative ions pass through a gas or a thin carbon foil and get stripped of their electrons to form positive ions.

The positive ions are then routed into a high energy (5-150 MeV/ion) mass spectrometer at which the more abundant carbon isotope current, i.e. ^{12}C and ^{13}C, are measured. After

the elimination of interfering ions via a dipole magnet and a Wien filter, ^{14}C ions are counted and relative isotopic ratio is determined. Finally, the measured isotopic ratio is compared to a known standard, such as the Australian National University (ANU) sucrose (=150.61 percent Modern Carbon (pMC) or 1.5061x13.56 dpm ^{14}C/gram Carbon).
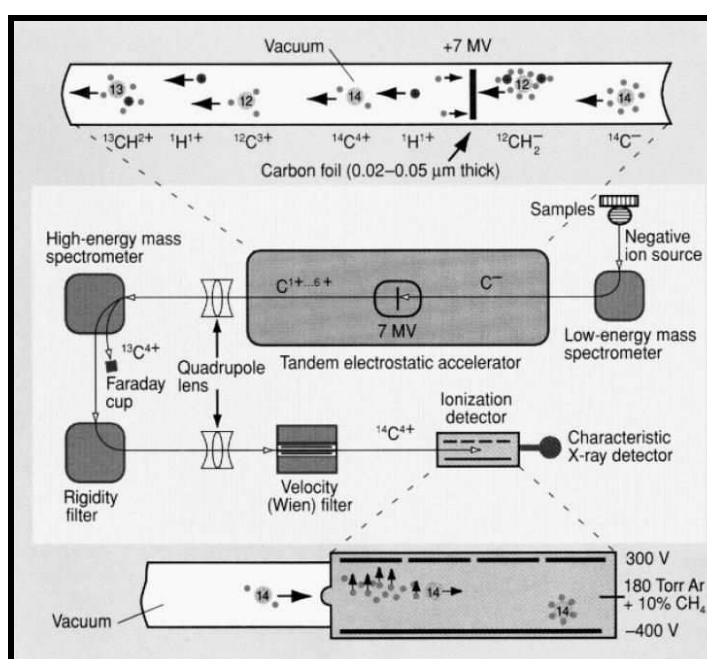
Figure 1.1 AMS system at Lawrence Livermore National Laboratory[17]

The AMS technique enabled the use of substantially lower radioactivity doses for biomedical applications, and the sensitivity levels obtained with this technique extended the radiocarbon dating to 50,000 years before the present (0.1% of Modern Carbon levels) [18]. However, AMS is limited in efficiency (~2%) and has strict sample preparation requirements. It doesn't provide any structural information for a molecule since it's only a very sensitive ion counting instrument. The motivation and the goal of

this thesis is to develop an instrument with comparable specifications of precision and sensitivity that can introduce a more cost effective solution for ^{14}C quantification and one that is versatile enough to be coupled with a liquid or gas chromatograph. The results described in subsequent chapters indicate that ICOGS is a competitive alternative to AMS. [19]

1.4.1 Isotope Ratio Analysis by Optical Methods

The new radiocarbon analysis technique described in this thesis is based on a combination of two well known high precision and high sensitivity laser spectroscopy methods, namely Optogalvanic Spectroscopy and Laser Intracavity Absorption Spectroscopy. These two optical isotopic ratio measurement techniques have already proven to be viable alternatives to Isotope Ratio Mass Spectrometry (IRMS) which has been the most widely used method to determine the abundance ratios of stable isotopes such as $^{13}C/^{12}C$ and $^{18}O/^{16}O$. In addition to wide uses in fundamental physics and metrology studies, laser based spectrometry is the method of choice especially for *in-situ* applications in environmental and biomedical sciences since IRMS is bound to laboratory operation involving tedious sample preparation steps that limit the analysis time per sample with high operating costs. [20-23]

In general, optical methods for isotope ratio measurements are based on resolving molecular spectra, mainly in the infrared region of the electromagnetic spectrum. Since the discrete energy levels associated with the rotational and vibrational motion of the molecules varies for isotopes of the same molecule, resonant laser interaction can be utilized for high-resolution isotope ratio spectrometry. The intensity of the spectral lines

obtained can be interpreted as a measure of the concentration of the absorbing species.
[24]

The direct way of determining the relative absorption of the molecules is done via measuring the transmittance of a sample as the incident laser light intensity is monitored while being tuned across a range of frequencies relevant to the analyte under study. The analyte concentration is directly related to absorbance (α) and Beer-Lambert Law of absorption [Eq. 1.1] gives the relation between the % transmittance of light and absorbance.

$$\frac{I_t}{I_0} = e^{-\alpha(\nu)} \tag{1.1}$$

Absorbance is a dimensionless quantity and it is given by the relation:

$$\alpha(\nu) = \sigma(\nu).n.l \tag{1.2}$$

Here, $\sigma(\nu)$ denotes the absorption cross section of resonant molecules and has units of area, n represents the concentration of molecules per unit volume and l is the effective path length along which the incident laser light travels across the sample cell. Absorption cross section is related to two important factors. One is the absorption line strength S which depends on the transition dipole moment and also on the population of energy levels which is temperature dependent. The other factor is the line shape function $f(\nu - \nu_0)$ where ν is the frequency of the incident light and ν_0 is the resonant frequency of molecules. It is determined experimentally and relies on molecular properties of the medium as well as the spectral resolution of the light source being used. Recent advances in laser and detector technology has enabled new and improved measurement techniques for direct detection of absorption. As implied by the equation [1.2], the method of choice

will be usually aimed at achieving high signal to noise ratios for detection of small losses due to absorption, and/or increasing the effective path length via cavity enhanced detection methods. However, none of these methods have achieved near the sensitivity and precision required for routine radiocarbon analysis. The highest sensitivity reported for carbon dioxide ratio analysis using cavity enhanced absorption methods is only 70 parts per billion (ppb) which is four orders of magnitude lower than the level required for analysis of natural radiocarbon [30].

Intracavity Absorption Spectroscopy (ICAS) and Cavity Ring-Down Spectroscopy (CRDS) are the two most sensitive methods for direct detection of absorption. In principle, they both introduce enhanced sensitivity by increasing the effective path length. In CRDS, the sample is placed inside an optical cavity with highly reflective mirrors. A narrow band laser pulse is sent into the cavity and as the beam reflects back and forth between the mirrors and travels through the sample, a small part of the beam is transmitted and the exponentially decaying laser power is monitored using a photodetector (Figure 1.2). The decay time for the cavity with and without the sample is measured as a function of the laser wavelength. Using the measured absorption coefficient and the cavity length information, the concentration of the sample is directly determined.
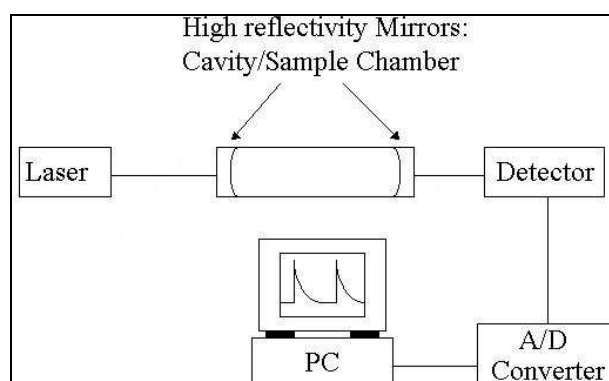
Figure 1.2 CRDS setup[25]

Similar to CRDS, ICAS is also a cavity enhanced absorption measurement technique but in this method the sample cell is placed inside the laser cavity (Figure 1.3). This configuration enables the system to be always on or close to resonance and does not require separate stabilization setup to achieve resonance conditions for sample cell. Also, with this configuration, optical feedback from the external resonator is avoided which is a possible drawback in some CRDS applications. The sample absorption spectrum is observed as dips over the broadband laser emission spectrum as the laser is tuned across its gain profile. The effective path length, L_{eff}, achieved with this technique can reach to $c.t$ where c is the speed of light, and t is the mode generation time of the laser. In practice, L_{eff} as long as 10^7 meters has been reported [22]. In principle, highest sensitivity with ICAS is achieved when the laser operates close to threshold. Under those conditions, small losses due to the presence of absorber is compensated with additional gain in the active laser medium. However, as it is the case in all methods that measure absorption directly, the lack of high quality tunable lasers relevant to radiocarbon analysis and more importantly because of the inability to measure power fluctuations as low as a few nano-

Watts, these techniques cannot achieve the sensitivity and precision required for quantification of natural levels of carbon-14 and compete with state of the art mass spectrometry techniques for isotope ratio analysis. [23-29]
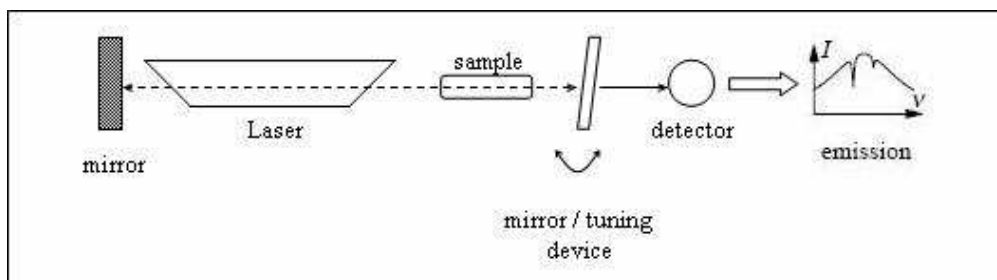
Figure 1.3 ICAS system for direct detection of absorption

1.4.2 Indirect Detection of Absorption and Optogalvanic Spectroscopy

Absorption spectroscopy, by itself, is not the proper spectroscopic method for routine radiocarbon analysis due to its limitations mentioned above. We now have developed a new technique based on multi-pass configuration of intracavity absorption and stimulated emission spectroscopy and used Optogalvanic Effect for trace level concentration measurements. In Optogalvanic Spectroscopy detection is electrical rather than optical. [31] When a low noise, RF excited gas discharge is irradiated by a molecule specific narrow-band gas laser, such as $^{14}CO_2$ laser, it changes the electrical properties of the discharge which can be detected with high sensitivity using relatively simple electrical circuitry. The amplitude of the electrical response is proportional to concentration of the absorber. With proper discharge conditions, this method enables high precision, specificity and accuracy for trace gas analysis. Throughout this thesis, detailed explanation will be given on how OG Spectroscopy has been implemented to quantify

attomoles of ^{14}C in submicrogram samples and how it may provide an alternative to complex mass spectrometers for routine radiocarbon analysis both in the field or in laboratories.

In the next chapter, we will give more details on the optogalvanic effect, including historical information for sensitive concentration measurements using this technique as well as physical models that explain OG effect. In Chapter 3, a detailed explanation of the experimental system and measurement procedures will be given and in chapter 4, we will explain the enhancement mechanism via intracavity setup and present the results of our measurements. In chapter 5, we will explain the non-linearties we observed throughout the calibration studies. We will also outline a rate equations model on the signal enhancement mechanism.

Chapter 2 :   Optogalvanic Effect As A Detection Tool

2.1   Overview

Radiocarbon analysis using laser spectroscopy with the sensitivity of an accelerator mass spectrometer requires a technique that doesn't rely on optical measurements. Because in order to detect molecules with only attomole concentrations, minimum detectable laser intensity change through the absorption path length must be of the order of nano-Watts which is not possible to achieve with today's technology. On the other hand, Laser Optogalvanic Spectroscopy (OGS) makes use of the Optogalvanic Effect (OGE) which is an electrical response of a gas discharge to a resonant laser interaction with an atomic or molecular transition of an analyte present in the discharge. The optical perturbation effects the equilibrium distribution of excited state populations which causes a modification in the electron energy distribution function. This effect leads to a change in the impedance of the discharge and can be detected, for example, as a voltage change across a ballast resistor in the driving power supply. Amplitude of the electrical response is directly proportional to density of resonant molecules. Therefore OGS introduces a sensitive detection method with high specificity and much less complexity than that of mass spectroscopy or laser absorption studies.

2.1   History and Applications

Earliest studies related to optogalvanic effect was made by Foote et al in 1925 [31]. Their experiments included optically excited caesium atoms and they observed increased ionization due to collisions with the excited atoms. Later in 1928, Penning made the first observations of OGE [30]. He worked with neon discharges and realized that the

emissions from one neon discharge lead to impedence changes in the adjacent neon discharge.

However, extensive research on OGE started after the invention of lasers. In 1964, Garscadden et al. observed an increase in the discharge current of a He-Ne gas laser as it went over the laser threshold [32]. In 1970, Skolnick used this laser effect on the discharge to stabilize the frequency of a CO_2 laser to the center of the laser power vs frequency curve [33]. His method was based on modulating the laser frequency using a piezoelectric transducer to change the cavity length and monitoring the impedance variations of the laser discharge tube. Using the fact that the change in the impedance is proportional to laser output power, he was able to stabilize the laser to the line center without the need for high quality laser power or wavelength meters.

An improved method for CO_2 laser frequency stabilization was reported by Shy et al [34]. They used optogalvanic Lamb dip to stabilize the laser frequency and achieved an estimated frequency stability of better than 100 kHz.

The first use of OGE as a sensitive spectroscopic tool was by Green et al. in 1976. They used a tunable dye laser to obtain high-sensitivity spectra of various species in a gas discharge and demonstrated OGS as a viable alternative to absorption and fluorescence spectroscopy [35]. After this pioneering work, Turk et al demonstrated the possibility of detecting trace levels of sodium concentrations in flames at the parts per billion level using laser enhanced ionization [36, 37].

The advent of high quality lasers together with the high sensitivity and precision introduced by the OGE has enabled high-resolution spectroscopic analysis of atoms and molecules with greater ease than conventional optical methods. [38, 39] In 1994,

Murnick et al reported a new method for ratio analysis of stable isotopes of carbon, namely $^{13}C:^{12}C$, using OGS [20]. They utilized molecule specific $^{12}CO_2$ and $^{13}CO_2$ gas lasers and obtained OG signals with phase sensitive detection. The sample was kept in an RF-gas discharge cell and contained 5% CO_2 in Nitrogen. The presence of N_2 in the discharge enhances the OG signal for the same reason a CO_2 laser output is increased by efficient energy transfer between electronically excited nitrogen molecules and upper laser level of CO_2. [40] Their results yielded a sensitivity of better than 10 parts per million and a dynamic range of over two orders of magnitude for CO_2 concentration.

Later in 1996, Murnick and his colleagues developed the first successful application of OGS as a rapid and low cost carbon isotope ratio analyzer to measure stable isotope ratios of carbon dioxide of exhaled human breath [41]. After the ingestion of ^{13}C labeled compounds, the exhaled breath, which contains about 5% CO_2 with nitrogen being the most abundant gas, is analyzed to determine the increase in $^{13}CO_2$ level above the patient's own baseline breath. The results of this non-invasive procedure are used in diagnosis of possible Helicobacter pylori infection which is known to be a cause for ulcers. The sensitivity and precision introduced with this technique made it possible for this instrument to be used in place of conventional isotope ratio mass spectrometers in hospitals and clinics across Europe and the United States [42].

In these studies, isotope ratios are reported in delta (δ) units as a part per thousand deviation from a standard and it is given by,

$$\delta(‰) = \left(\frac{R_{sa} - R_{std}}{R_{std}} \right) \times 1000 \qquad (2.1)$$

The ratios are determined by simultaneously measuring optogalvanic signals, *S,* from a cell that contains unknown samples, x, and a reference cell, std, and subsequently forming the double ratios;

$$\frac{^{13}S_x}{^{12}S_x} \bigg/ \frac{^{13}S_{std}}{^{12}S_{std}} \qquad (2.2)$$

This procedure greatly decreases the systematic errors due to fluctuations in laser power and wavelength and cancels out small discharge variations with time. They have achieved a limit of detection of about 0.5‰ for $^{13}CO_2$ which implies a sensitivity of about 5 ppm. Another application of OGE in high precision spectroscopy was demonstrated by Okil in 2004 [43]. In his dissertation work, he developed an isotope ratio analyzer to continuously monitor the variations in concentration and isotopic ratio of $^{13}CO_2$ and $^{12}CO_2$ in air. Carbon dioxide constitutes about 0.04% of air and natural abundance of $^{13}CO_2$ is 1.1%. In his experiment, outside air flowing slowly through an RF discharge cell was analyzed continuously for days and a sealed reference cell was used for continuous real time normalization. By careful system optimization and control procedures, CO_2 concentration variations as low as 0.1 ppm and $^{13}C:^{12}C$ variations of about 0.5δ were easily detected with a signal to noise ratio of about 2000. Under his experimental conditions, measurement sensitivity to 26 femtomole of $^{13}CO_2$ in 734 nanomoles of CO_2 or about 5 ppm was demonstrated.

In summary, OGS introduces several advantages over mass spectrometric methods and other optical methods for isotope ratio analysis. As a less complex and robust detection method, it can be further improved from the above mentioned studies for direct radiocarbon analysis at the part per trillion level or better.

2.3   Optogalvanic Effect in CO_2 RF Discharge

In principle, Optogalvanic Effect refers to a change in the impedance of a gas discharge due to absorption or emission of radiation. The optical perturbation alters the equilibrium distribution of the excited species which changes the collisional rates between the electrons and the molecules. This in turn causes a change in the discharge voltage or current which can be easily measured with high precision and accuracy. Below saturation, this electrical signal is proportional to laser intensity, the area of the laser beam, optical path length across the discharge and the density of the interacting species. Having the CO_2 molecules in a glow discharge medium ensures significant populations in the excited rotational-vibrational states. Using a narrow band, molecule specific CO_2 laser in resonant with one of the rotational-vibrational transitions, high-resolution isotope ratio analysis is performed with much less complexity compared to optical or mass spectrometric analysis techniques. Since the response is electrical in nature, the signals can be amplified with appropriate circuitry and averaging techniques can be used to achieve high signal to noise ratios.

2.3.1   Mechanisms of the Optogalvanic Effect

The experiments presented in this work utilize a low pressure glow discharge generated by radio frequency power supply. Although these types of discharges have found widespread use in fundamental research and practical applications [44, 45] due to the complexity of the physical processes in the plasma, different models are developed for optogalvanic signal generation in atomic or molecular systems. One of the explanations associate the OG signal with the laser induced change in the ionization balance of the glow discharge [46]. According to this model, the laser irradiation causes the metastable

atoms to be excited to levels with higher or lower ionization probability thus changing the ionization rates which in turn leads to a measurable change in the impedance of the discharge. This model is generally used to explain the optogalvanic effect in the atomic discharges in which the energy difference between the higher laser level and the ionization threshold is relatively small.

However, in molecular discharges, such as the CO_2, there are several low lying rotational-vibrational energy levels far below from the ionization threshold. While the ionization potential for the CO_2 molecule is 13.77 eV, the resonant laser interaction energy is of the order of 0.1 eV. According to Moffatt and Smith [47], the OGE signal is generated as a result of a change in the equilibrium temperature of the gas discharge as the laser perturbation induces new excitation or de-excitation pathways via absorption or stimulated emission. The induced transition changes the gas number density in the irradiated part of the discharge which alters the collisional frequency between the electrons and the molecules without effecting the ionization rates. The variation in the mobility of the electrons leads to a change in the impedance of the discharge which can be detected with great sensitivity in the form of a change in the voltage or current of the discharge.

The relevant rotational-vibrational energy levels of the CO_2 molecule has been studied in great detail especially in the context of the operation of a CO_2 laser [48, 49]. The contents of the sample cell we use in our experiments are similar to that of a CO_2 laser and contain either pure CO_2 or CO_2-N_2 gas mixture. Figure 2.1 shows the relative energy scales of the vibrational modes of $^{12}CO_2$ and N_2 molecules together with the excitation and de-excitation pathways into these modes. Large isotope shifts in the vibrational-

rotational spectra of the CO_2 molecule, enabled the development of various carbon dioxide isotope lasers and thus far approximately 1500 different lasing transitions have been determined with high spectral purity [58]. In this work we make use of $^{12}CO_2$ and $^{14}CO_2$ isotope lasers whose emission line centers are well separated in wavelength from each other and also from that of the other more abundant $^{13}CO_2$ isotope.
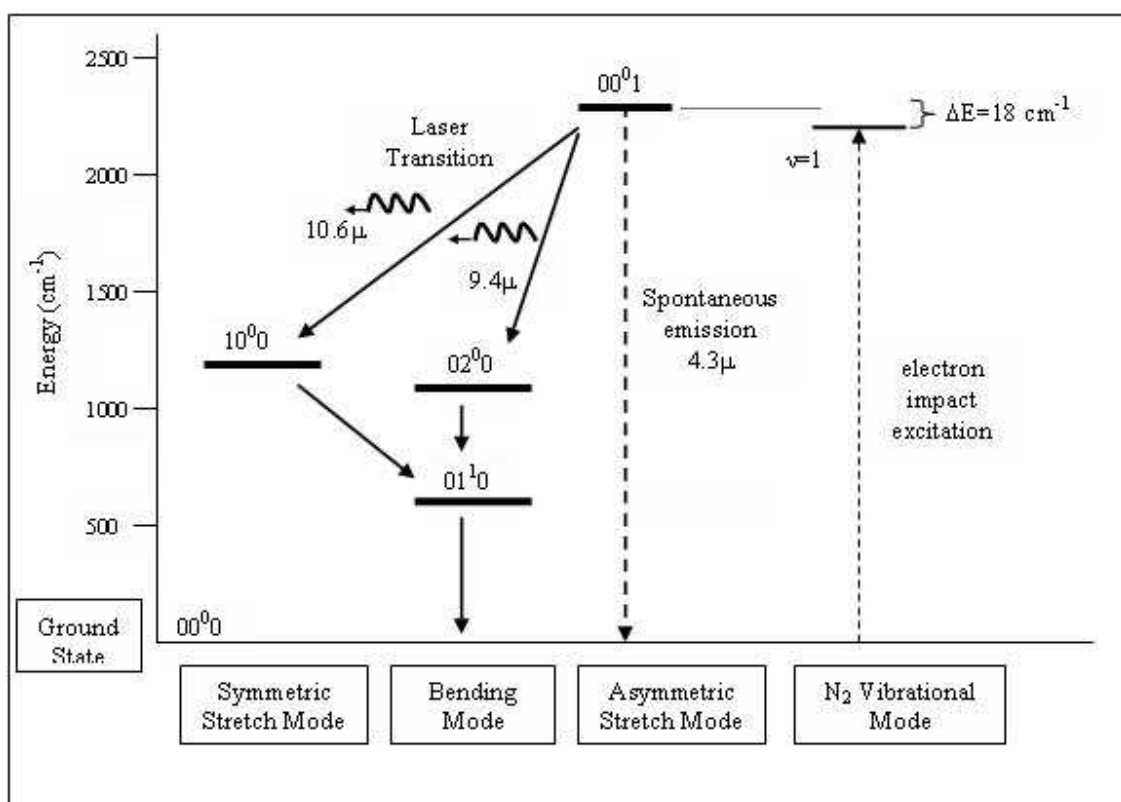
Figure 2.1 The vibrational energy level diagram for 12CO2 laser transitions together with the excitation and de-excitation pathways

Associated with each vibrational level there are a series of quantized rotational energy levels of the molecule (Figure 2.2) which are designated by their rotational quantum number J. At thermal equilibrium, distribution of these rotational modes follow the Maxwell-Boltzmann distribution:

$$N_\nu(J) = N_0 \cdot (2J+1) \cdot e^{-E_J/kT}$$

Here, the rotational energy (E_J) is given by the relation $E_J = hcB_eJ(J+1)$ where B_e is the rotational constant which is inversely proportional to the moment of inertia (I) of the molecule as given in the relation; $B_e = h/4\pi cI$. For a CO_2 molecule, $B_e \sim 0.39$ cm^{-1}.
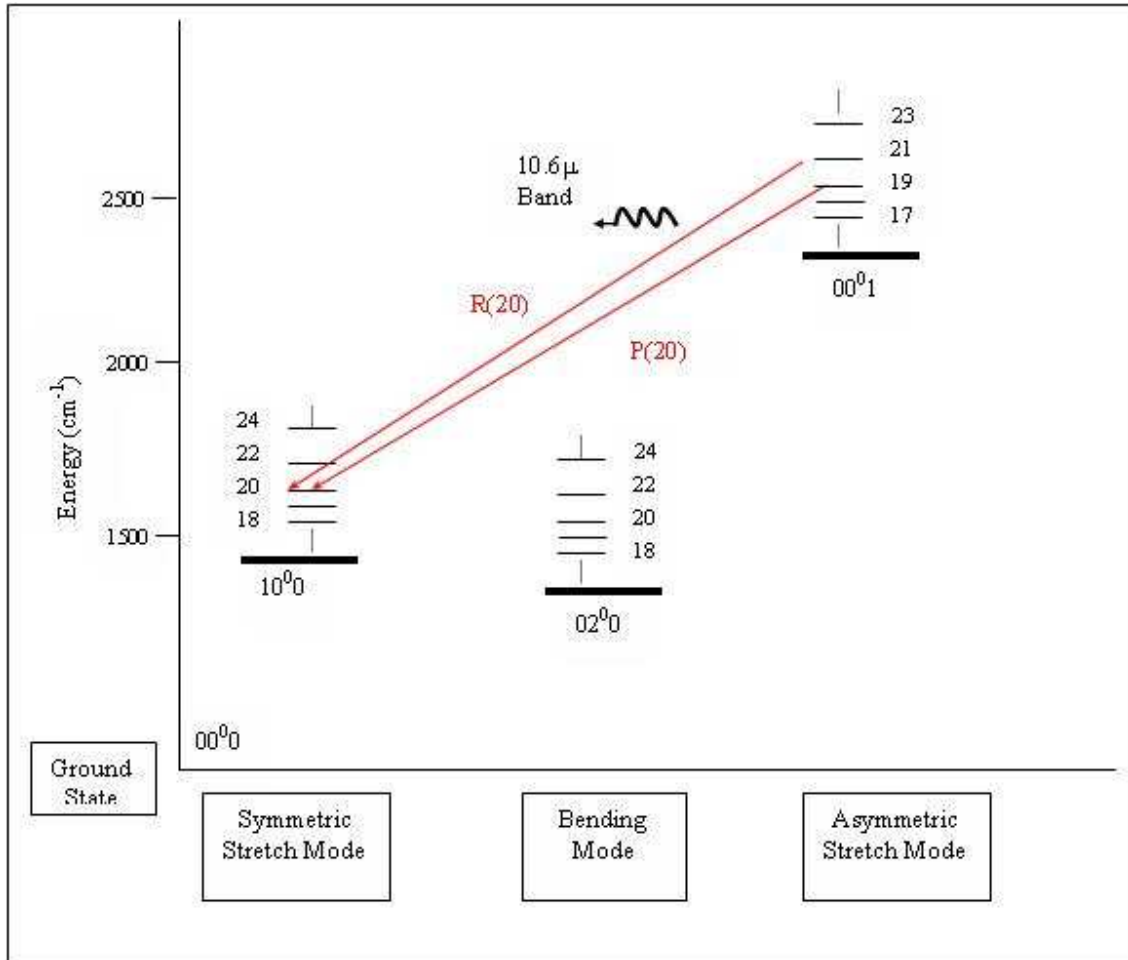
Figure 2.2 Energy level diagram of the rotational levels of CO_2 molecule are shown with the vibrational levels and laser transitions for the 00^01-10^00 band

Energy level diagram of the rotational levels of CO_2 molecule are shown with the vibrational levels and laser transitions for the 00^01-10^00 band In a CO_2 laser, lasing transitions occur between two rotational levels that belong to the two different vibrational

modes. According to selection rules, only the transitions whose rotational quantum numbers change by +1 or –1 are allowed. Transitions from *J to J*+1 are called P-Branch lines and those from *J* to *J*–1 are called R-Branch lines. Patel has demonstrated that the P(20) is the dominant transition in a CO_2 laser [41, 56]

Efficient excitation of the ground state CO_2 molecules to upper laser level is achieved by rapid energy transfer from nitrogen molecules which are excited to their metastable vibrational level via electron impact excitation. From this point, the following energy transfer processes occur which are also the relevant mechanisms that can cause the gas temperature to increase or decrease that give rise to OGE signal [50,51]:

1) $CO_2(00^01) + M \rightarrow CO_2 (nm^lo) + M + T$

2) $CO_2 (00^01) + h\nu (10.6\mu) \rightarrow CO_2 (10^00) + 2h\nu (10.6\mu)$

   $CO_2 (10^00) + M \rightarrow CO_2 (01^00) + M + T$

   $CO_2 (01^00) + M \rightarrow CO_2 (00^00) + M + T$

3) $CO_2 (00^01) + M \rightarrow CO_2 (00^00) + h\nu (4.3\mu)$

The first process describes the relaxation from the upper laser level due to intermolecular collisions in the absence of incident resonant radiation. Here M stands for a possible collision partner and it can be CO_2, N_2 or CO which may be produced by the dissociation of the CO_2 in the discharge. As a result of this process, the excess energy form the de-excited CO_2 molecule from the asymmetric stretch mode is released to the discharge as translational kinetic energy, T. The collisional decay time from the upper laser level in a typical CO_2 laser system is about 0.4 ms.

The second process is the relaxation of the CO_2 molecule from the upper level due to stimulated emission induced by the incident resonant laser radiation. The lower laser levels (10^00) and (02^00) are essentially resonant with an energy difference much less than kT. From these levels, the molecule makes a quick transition to (01^10) level as a result of intermolecular collisions releasing more translational kinetic energy. This level is essentially metastable and also has a high probability of thermal excitation from the ground state. Therefore collisional de-population of this level is critical for CO_2 molecules to be able to reach to ground state so they can be excited back up to their first excited state. In a CO_2 laser system, this process has a lifetime of about ~ 70 μs.

The third mechanism that may lead to de-population of the upper laser level is the spontaneous emission process from the (00^01) level to the (000) ground state of the CO_2 molecule. The natural lifetime of this level is determined to be around 2.4 ms [57].

According to the temperature model of the OGE, the energy that would be lost via process (1) or (3), namely the vibrational-vibrational-translational (*V-V-T*) or the vibrational-translational (*V-T*) processes, is alternatively lost by the stimulated emission process described above. Depending on wheather the system is in the absorptive or gain mode, OG signal can either be positive or negative which implies a cooling or heating of the gas discharge. [50, 51]

In our experiments, the sample is in a low power (2 to 5 W) RF glow discharge which maintains the population of excited states in equilibrium. When the RF field is applied, primary electrons between the electrodes are accelerated and they collide with molecules

exciting them to their upper vibrational levels. The conductivity of the plasma is given by [53]:

$$\sigma = \frac{e^2 n_e v_m}{m(\omega^2 + v_m^2)} \tag{2.3}$$

Here, n_e is the electron density and ω is the angular frequency of the RF field. In the limiting case where the collision frequency (v_m) is much greater than the angular frequency of the RF field, the equation reduces to $\sigma = e^2 n_e / m v_m$. The conductivity is then proportional to the mobility of the electrons which is defined by the relation:

$$\mu_e = e / m v_m \tag{2.4}$$

The collision frequency (v_m) is given by

$$v_m = n_g \upsilon_d \sigma_m \tag{2.5}$$

where, υ_d is the drift velocity of the electrons and σ_m is the collision cross section. υ_d can be determined from the average kinetic energy of electrons in the discharge. For the system under study where the applied RF voltage is about 800 Volts and the mean free path of the electrons is $\sim 0.32 \times 10^{-4}$ m at 310 K temperature, the drift velocity of the electrons is $\sim 6.4 \times 10^7$ cm/sec.

The electron density (n_e) can be obtained by using the relation for current density, which is given by:

$$j = -e n_e \upsilon_d \tag{2.6}$$

At the pressure around 1 Torr used in our system, the density of the neutral molecules ($n_g \sim 3.5 \times 10^{16}$ cm^{-3}) are much higher than the electron density ($n_e \sim 2.27 \times 10^8$ cm^{-3}),

therefore the distribution function of the charged particles is affected significantly by their collisions with the molecules.

In practice, the optogalvanic signal is generated as a result of the resonant laser beam perturbing the population of the excited molecular states in the discharge which in turn changes the collision rates and the mobility of the electrons. The change in the conductivity of the discharge is measured in the form of a change in the discharge current or voltage. When a laser of intensity $I(v)$ is incident on the gas discharge with similar characteristics mentioned above, the optogalvanic signal, S, can be expressed as an integral over the interaction space as follows:

$$S = \int_0^L dz \int_0^R rdr \int_0^{2\pi} d\theta[n(r,\theta)I(r,\theta,z,v)\sigma(v)K] \qquad (2.7)$$

Here, n is the number density of the interacting species, $\sigma(v)$ is the stimulated emission or absorption cross-section and K is an optogalvanic proportionality constant which is a complicated function of the discharge conditions and the rates associated with various interactions within the gas discharge. Below saturation and under the conditions where K is independent of n, the signal can be approximated by:

$$S = nLIA\sigma K \qquad (2.8)$$

Where L is the laser-discharge interaction path length, I is the average laser intensity in W/cm^2 and A is the average area of the incident laser beam.

As implied by the equation, detection of trace amounts of molecules such as contemporary or sub-contemporary levels of $^{14}CO_2$, will require increased laser intensity, longer interaction length and/or determining the optimum discharge conditions for proper

optogalvanic proportionality constant, all within the limits of our system. For this purpose, the new spectroscopic method described throughout this work utilizes cavity enhanced detection techniques mentioned in the preceding chapter. The new standing wave technique reported here is analogous to, but with key differences from the Intracavity Absorption Spectroscopy (ICAS). The most significant difference from ICAS is that detection is via the optogalvanic effect rather than optical. In addition, the analyte in this case is the same as the lasing species and also an optogalvanic signal exists for stimulated emission or absorption.

Chapter 3 :   Experimental Setup And System Optimization

3.1   Overview

Laser assisted isotopic ratio analysis of stable and naturally abundant isotopes of carbon for breath analysis and environmental monitoring were successfully demonstrated by Murnick et al. and Okil [41, 43]. The goal of this work is to develop a new ultra-sensitive laser based technique to quantify the ^{14}C content in submicrogram samples that may replace large accelerator mass spectrometers for variety of applications. This implies an improvement of more than six orders of magnitude in detection sensitivity from previous work. In this chapter, a detailed explanation of experimental design as well as the steps taken to optimize the system is presented.

3.2   Experimental Design

The system components of the ultra-sensitive radiocarbon analyzer developed in this work is schematically shown in Figure 3.1. The analyte cell is placed inside the $^{14}CO_2$ laser cavity designated by M1, high reflective mirror and grating, and M2, 85% reflective output coupler. The DC excited $^{14}CO_2$ laser is custom made by the LTG Lasertech Group, Inc. with its cavity extended to accommodate the sample cell. The 165 cm long resonator is built with 4 invar rods for their low thermal expansion coefficient. Single laser line selection such as P(20) or R(20), which correspond to 11.768 μ and 11.344 μ respectively, is achieved by the grating while the piezo-electric crystal fitted at the front mirror, controlled by a PZT driver, enables further fine tuning of the laser. The sealed laser tube has a glass jacket for water cooling and the temperature stabilization of the laser around 9 ^{o}C is achieved via a Neslab water chiller.

The experimental system also includes a small $^{12}CO_2$ laser (Synrad model 48-1) for normalization. This laser operates at 10.6 μ and the emission is in resonance with only $^{12}CO_2$ molecules in the cell. Taking advantage of the partial transmittance of the front mirror of the $^{14}CO_2$ laser, about 1.5 W of 10 W $^{12}CO_2$ laser beam is incident onto the intracavity sample cell. Due to high abundance of $^{12}CO_2$ in the analysis cell, the $^{12}CO_2$ OG signal does not need to be enhanced via another ICOGS setup and can be measured in a typical external cell configuration. Both lasers are modulated at different frequencies and $^{12}CO_2$ and $^{14}CO_2$ signals are acquired simultaneously by phase sensitive lock-in technique, which will be explained in the upcoming sections. The $^{14}CO_2$ laser is modulated with an SR540 optical chopper manufactured by Stanford Research Systems, Inc. On the other hand, $^{12}CO_2$ laser is chopped electronically via the gating signal generated by the computer and sent to the Synrad UC-1000 laser controller.
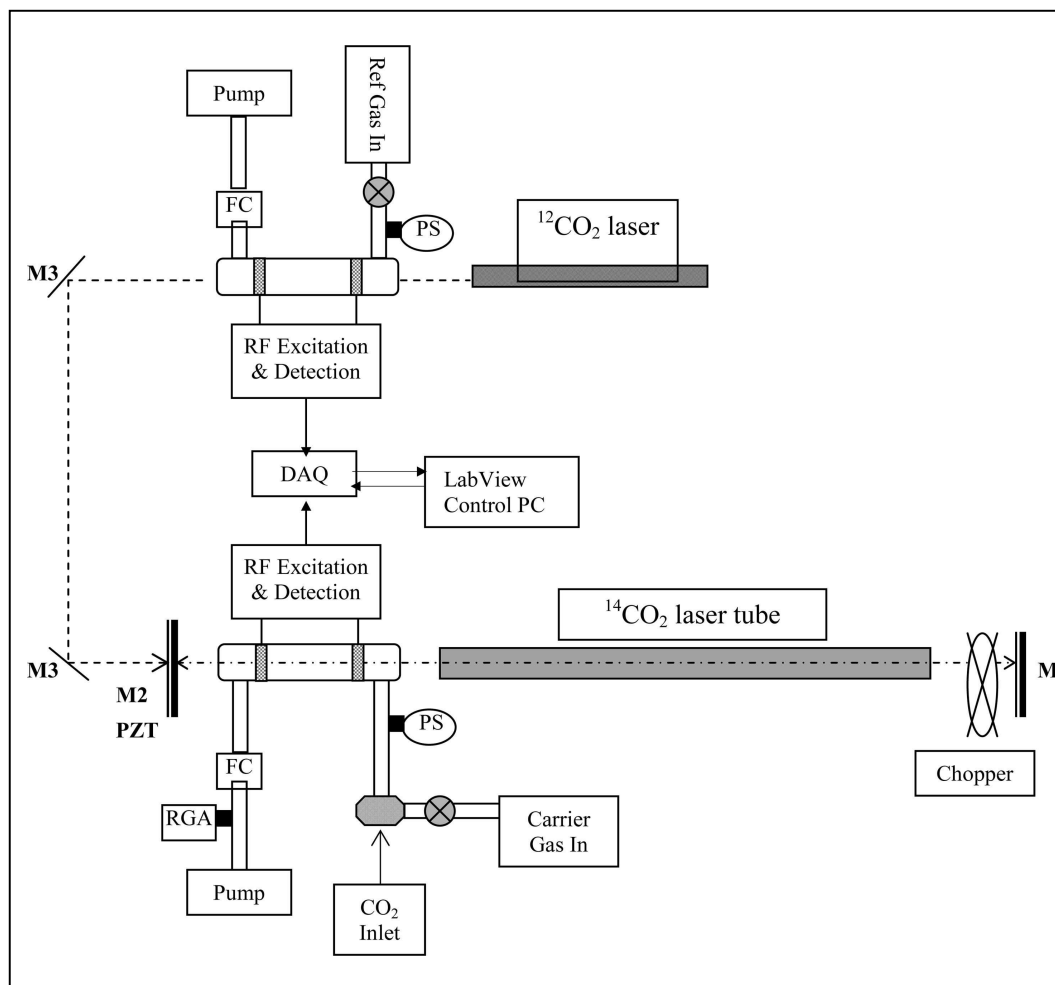
Figure 3.1 Experimental Setup of ICOGS for high sensitivity radiocarbon quantification. The OGE cell inside the cavity has Brewster windows to reduce losses. The C12 laser incident on the intracavity cell provides a "C12 signal" that is used for normalization of the C14 signal. The chopper inside the laser cavity is for modulating the $^{14}CO_2$ laser. M1, high reflective mirror and grating; M2, 85% reflective output coupler; M3, gold plate mirror; PS, pressure sensor; FC, flow controller; RGA, residual gas analyzer; DAQ, data acquisition board

3.3   Discharge Excitation and Optogalvanic Signal Detection

In ICOGS, population of excited state molecules is maintained in a glow discharge. In our experiments, the analysis cell is capacitively coupled to tunable, low power (~5 W) RF oscillator circuitry that initiates and sustains the discharge. This is the preferred method for operating at low pressures (1 to 5 Torr) as it helps minimize pressure broadening for high-resolution spectroscopic analysis. [43, 62] As it will be explained in the subsequent chapters, higher sensitivity with $^{14}CO_2$ analysis has been achieved by lowering the pressure, within the limitations of the excitation system, thereby lowering the non-resonant background contributions from $^{12}CO_2$ and $^{13}CO_2$. Furthermore, since the glow discharge is generated via the RF voltage applied to the electrodes mounted outside the analysis cell, the electrodes do not come into direct contact with the samples being analyzed, preventing possible contamination. (Figure 3.2)
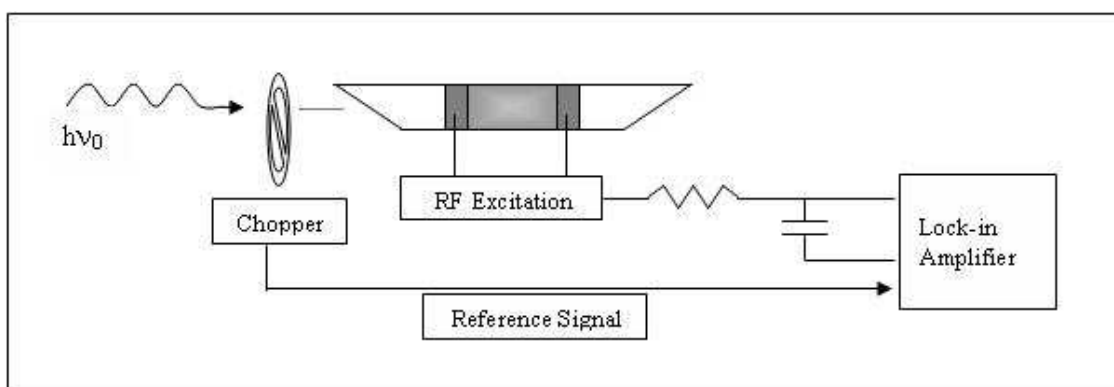
Figure 3.2 Basic Optogalvanic Signal Detection Scheme. Specificity is achieved by a modulated resonant laser beam incident on a glow discharge. OG response is detected as a change in the impedance of the discharge. The signal is filtered and captured by phase sensitive detection method

In practice, the power supply to the discharge is kept at a constant voltage and as the periodic resonant laser perturbation alters the mobility of the charge carriers, and

therefore the impedance of the discharge, an amplified current at the collector-emitter junction of the RF transistor is measured as a periodic voltage change across a ballast resistor at the chopping frequency of the laser [62]. This optogalvanic signal output is then fed into a differential amplifier board where the signal is filtered from high frequency and the DC components, amplified and sent to the computer or lock-in amplifier for data collection and analysis.

3.4   Data Collection and Processing

Throughout our experiments, optogalvanic signal is captured and processed using a computer that includes a Data Acquisition (DAQ) Board and a program developed in LabView programming language. The DAQ Board is a 16-Bit National Instruments NI-6120 Simultaneous Sampling board and the interface between ICOGS and the board is made possible by a National Instruments BNC-2110 interface with BNC connectors for analog and digital I/O connections. The DAQ board has 4 analog input (AI) channels and each channel has it's own analog-to-digital converter. This property of the board enables sampling of the OGS from two cells at the same time, as opposed sequential sampling of each channel, eliminating the down time per channel, thereby eliminating possibility of losing data points throughout the duty cycle of the laser modulation. First two AI channels are dedicated to OGS acquisition from external reference cell and internal sample cell, respectively, while the other two channels are assigned to collect data from the pressure sensor and laser power meter or the laser exciter OG output. The data acquisition is initialized by the trigger signal from the mechanical chopper of the $^{14}CO_2$ laser. As the laser modulation frequency is manually set using the adjustment knob in the front panel of the chopper controller, the same frequency is entered as an input in the

front panel of the program. $^{12}CO_2$ laser is electronically chopped by the TTL signal from the digital counter output which is also entered by the user from the front panel of the program. Data sampling rate is chosen to be the multiple of the two chopping frequencies and number of samples per second is chosen to be equal to sampling rate. This way it is ensured that data acquisition for two different frequencies is synchronized throughout the one-second averaging time. A typical optogalvanic response to a periodically modulated laser beam is shown in Figure 3.3.
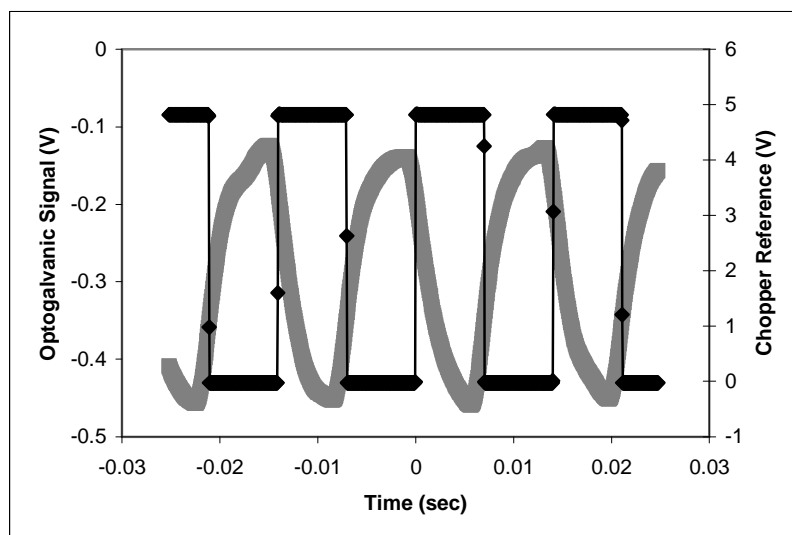
Figure 3.3 Example of an OG signal in response to a laser modulated at 71 Hz and averaged over 5 seconds. The sample is pure CO_2 gas flowing at 0.05 ml/min with 0.97 Modern enrichment.

From each cell, waveforms for $^{14}CO_2$ and $^{12}CO_2$ optogalvanic response are captured at each second and a fast fourier transform (FFT) algorithm is executed to measure the signal amplitudes at fundamental modulation frequencies. This one second averaged value is then saved for offline data analysis as well as used in the real time laser stabilization routine.

3.5   Laser Frequency Stabilization

Optogalvanic signals have been widely used to actively stabilize the frequency of cw CO_2 lasers [31, 63, 64]. Long term laser stability is mainly effected by variations in the laser cavity length due to temperature fluctuations. Changes in the cavity length causes drifts in laser power and resonant line center operation. To compensate for these drifts, the output coupler of the $^{14}CO_2$ laser and the back mirror of the $^{12}CO_2$ laser are mounted on a piezo-electric transducer that is used for dynamic adjustment of the cavity length. For experiments that require long term stability of the system, computer controlled feedback algorithm monitors the optogalvanic signal from a reference source such as the external sealed cell and/or from the $^{14}CO_2$ laser itself and automatically adjusts the PZT voltage to compensate for the drifts in laser cavity. The algorithm first determines the peak signal amplitude or laser power by sending a ramp voltage output to both PZT power supplies independently. After completing a scan through the full range of the PZT, the Labview program sets the PZT driver output voltage to the corresponding highest optogalvanic signal or highest laser power and actively monitors and compensates for the drifts from the peak amplitude by adjusting the PZT voltage.

In our experiments, we used an external sealed cell that contains 5% CO2 gas in air at 5 Torr with contemporary levels of radiocarbon. $^{12}CO_2$ laser stabilization is achieved by monitoring the OG signal acquired from this cell, while stabilization of the $^{14}CO_2$ laser is achieved by monitoring the OG signal obtained from the laser tube itself. Periodic modulation of the $^{14}CO_2$ laser causes a voltage change across a ballast resistor inside its own power supply which makes it possible for us to use this as a reference signal to stabilize the wavelength and also use it for laser power normalization. Figures 3.4 and 3.5

show the results obtained after implementing the feedback algorithm for stabilizing the lasers using optogalvanic effect. Left hand side of the curves represent the OG signal profile acquired by ramping the transducer across it's full range, namely 0 to 75 Volts and 0 to 1000 Volts for $^{12}CO_2$ and $^{14}CO_2$ lasers, respectively. Since the OG signal is proportional to laser power, computer controlled peak find and stabilization algorithm enables active long-term control of the lasers.
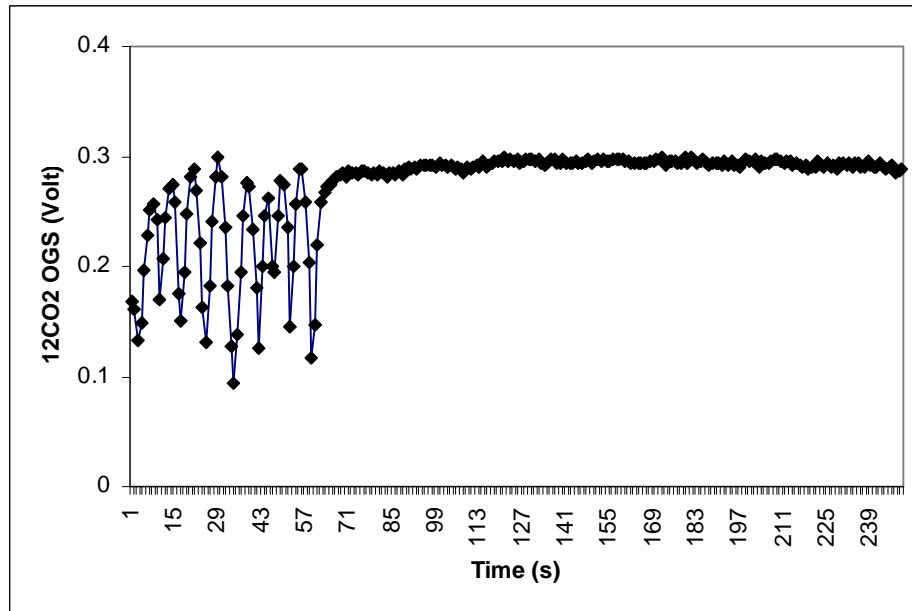
Figure 3.4 After completing a $^{12}CO_2$ OGS scan profile, computer locks the PZT voltage to make the laser operate on the highest peak of the signal and maintain stable operation. Variations in the signal with the present system is of the order of 1%.
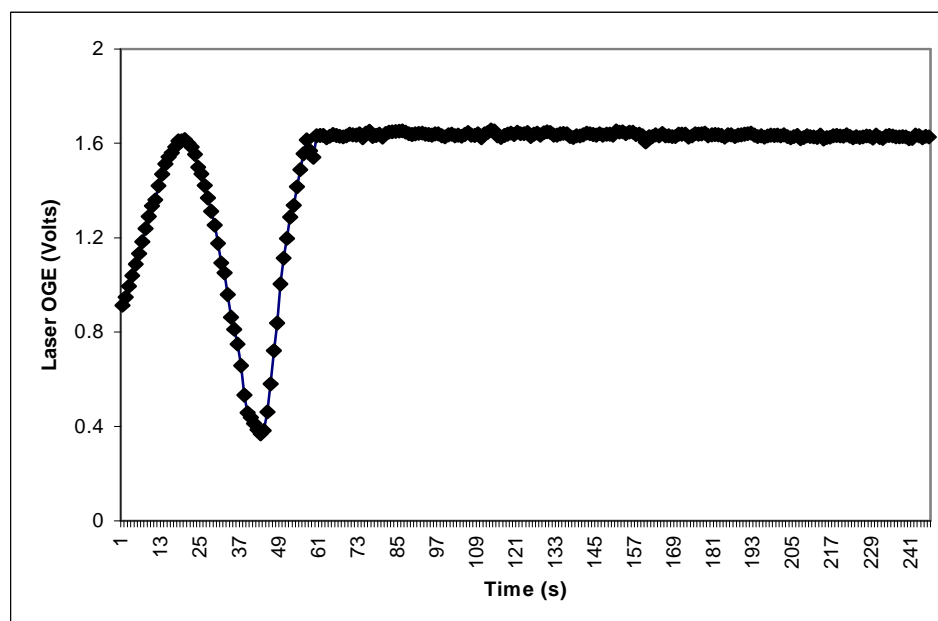
Figure 3.5 Following $^{14}CO_2$ Peak OGS scan across one FSR of the laser, computer stabilizes the laser on maximum of the laser gain profile. Variation in the signal after stabilization is about a fraction of a percent.

3.6   Internal and External Analysis Cells and Sample Introduction Methods

The intracavity analysis cell has a volume of about 9 ml and it is made out of quartz. The

cell windows are made of AR coated ZnSe material and they are mounted at the

Brewster's angle to minimize the cavity losses. CO_2 samples are introduced via the inlet

port of the cell as shown in Figure 3.1. The gas pressure is monitored by an MKS

Baratron (capacitance monometer) pressure transducer and the steady flow of gas is

achieved by an MKS flow controller (FC) while the system is being pumped down by a

Leybold turbo pump backed by a Leybold roughing pump. The cell is maintained at the

desired pressure by carefully adjusting the valve mounted on the outlet port of the cell. In

line with the pumping system there is a compact Residual Gas Analyzer (RGA) (Extorr,

Inc. Model XT 100). This compact RGA includes a Pirani gauge and an ion gauge for

low-pressure measurements and utilizes a quadrupole gas analyzer to measure the partial pressures of the residual gasses flowing out of the analysis cell. It is controlled by it's own software and mass scans are displayed on the computer screen. This instrument has proven to be very useful in verifying the contents of the sample vials being analyzed, in determining the residual gases such as water vapor or CO_2 that may be present in the system before introducing a new sample and also detecting possible sources of leaks in the plumbing system.

The external reference cell is a cylindrical sealed cell of about 10 cm long and 2 cm diameter. It contains 5% CO_2 in air at 5 Torr with natural level of radiocarbon. For a an isotope ratio analysis system with sub-delta precision, external cell can be filled with highly enriched radiocarbon in Nitrogen buffer so that OG signals can be detected without the requirement of an intracavity enhancement. As mentioned in Chapter 2, measuring the OG signals simultaneously for both cells and taking the double ratio of signals help eliminate systematic errors due to laser fluctuations and increase the precision of the system. For the present system, $^{12}CO_2$ normalization is achieved by the OG signal from the external cell, while the $^{14}CO_2$ is normalized to OG signal from the laser tube itself and pressure of analysis cell when pure CO_2 is used as the carrier gas.

3.6.1   Sample Introduction Methods

Radiocarbon analysis using mass spectroscopy methods, such as AMS, is based on measuring ion currents and involves complex sample preparation steps. These steps include pre-treatment of the sample for removal of contaminants and isolating from the matrix, combustion or acid hydrolysis procedure for carbon dioxide production and

finally the reduction of the sample to elemental carbon in the form of graphite in special hydrogen and iron powder reactors. [66] AMS measurements require samples to be at least 1 mg to obtain sufficient ion currents for analysis, therefore "dead carbon", i.e. graphite that is void of radiocarbon, is added as carrier which introduces new sample preparation steps.

On the other hand, ICOGS, which is based on the molecule specific, resonant optogalvanic signal, does not involve complex sample preparation steps and samples as small as micrograms can be analyzed with precision and sensitivity comparable to that of AMS. The only sample preparation steps for ICOGS are oxidation to CO_2 and the removal of water vapor. In his thesis work, Okil has demonstrated that an increase in water vapor content in the cell lead to an increase in the optogalvanic signal, reaching a peak around 10 to 15% relative humidity [43]. Although this leads to increased SNR as a result of increased signal, the water vapor content greatly varies from sample to sample, therefore it's now preferred to remove the water vapor completely before the measurement process. Another important advantage of ICOGS over ion counting methods is that this technique is non-destructive to samples and after each measurement they may be retrieved for further analysis, if desired.

Experimental setup of ICOGS provides versatility so that depending on the application, different operating procedures can be utilized for sample introduction. For biochemical applications where rapid analysis of 10 to 100 Modern samples with high throughput is required, flow through system can be used, whereas batch mode measurement procedure can be used for improved precision for analyzing samples with 1 Modern or less enrichment. These procedures are explained in greater detail in the following sections.

3.6.1.1 Batch Mode Measurement Procedure

This mode of operation involves the cell to be filled with either pure CO_2 sample or with CO_2-N_2 mixture and closing the valves to trap the gas in the analyte cell for batch mode measurements. This makes it possible to improve the precision of the system by performing longer time averaged measurements.

One possible drawback of this mode that we have experienced is the "memory effect" that may cause repeatability problems and usually larger signals especially for samples with low enrichments. Throughout this work, the samples are analyzed in only two different intracavity analysis cells. In pure nitrogen discharge, it was observed that residual CO_2 molecules from previous experiments come off the cell walls after turning on the discharge. (Figure 3.6) Therefore, after each measurement, especially after analyzing samples with enriched radiocarbon, the analysis cell needed to be baked with a heating tape and pumped down using a turbo pump to avoid memory effect in the subsequent measurements. Flushing the system with an inert gas such as N_2 for several hours was also found useful in cleaning the cell.
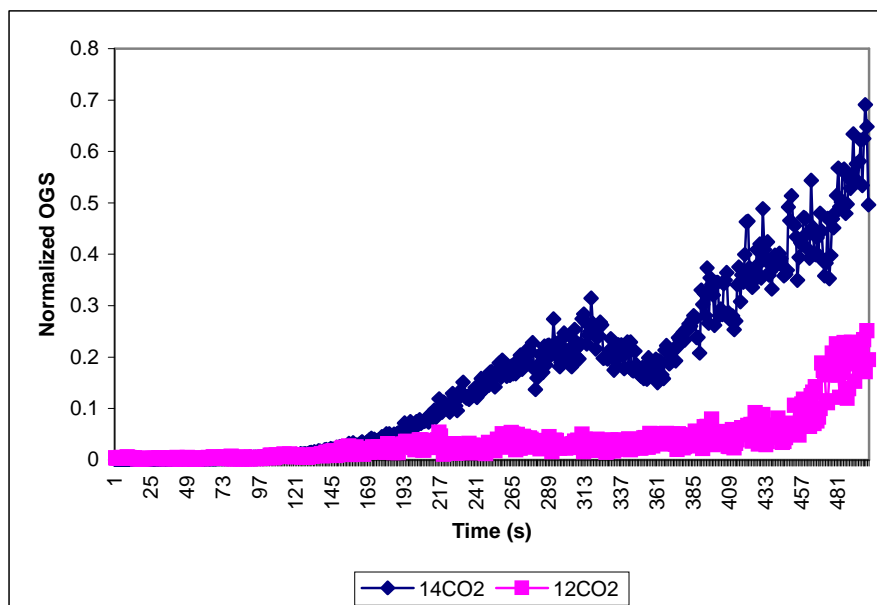
Figure 3.6 After the initiation of 5 Torr pure N_2 discharge, normalized $^{12}CO_2$ and $^{14}CO_2$ OG signals verify the increase in the CO_2 content in the cell.

3.6.1.2   Flow Mode Measurement Procedure

Another method used for sample introduction is the injection of pure CO_2 sample onto a constant stream of carrier gas which can be pure nitrogen, CO_2 stripped air or "dead CO_2" i.e. CO_2 gas that is void of radiocarbon. This type of sample introduction is similar to that of a mass spectrometer coupled with a Gas or Liquid Chromatography instrument [59,60]. In this operation mode, instead of the two port cell, a single port analysis cell together with a 0.32 mm ID quartz capillary tubing (Supelco, Inc) was used. (Figure 3.7). By using capillary tubing, the expansion volume was kept small enabling us to use smaller samples throughout the experiments. Pure CO_2 samples with varying $^{14}CO_2$ concentrations were introduced onto the stream of carrier gas flow using a gas tight syringe via the septa as shown in the figure.
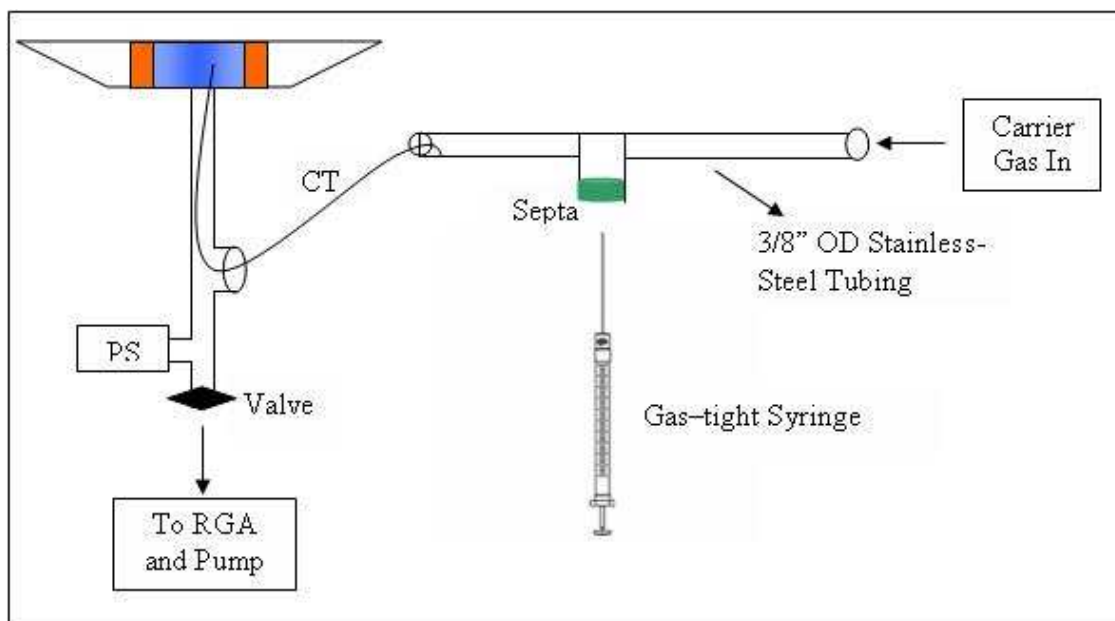
Figure 3.7 Schematic of sample introduction via injection. 2 ml or less gas sample is injected into a volume of about 40 ml. Cell pressure is kept around 5 Torr while the flow is adjusted via the valve. PS: Pressure Sensor, CT: Capillary Tubing

One set of experiment with the continuous flow mode for 1ml CO_2 injected into a stream of CO_2-free air as a carrier gas is shown in Figure 3.8. As the sample flowed into and out of the analysis cell, the transient signals were recorded simultaneously for both $^{14}CO_2$ and $^{12}CO_2$ resonant laser interaction with corresponding isotopes. In the subsequent chapters, injection experiments will be analyzed in greater detail with their relevance to calibration of the system and studies on modeling of physical mechanisms of observed saturation effects with increasing radiocarbon concentration, as shown in the inset of the figure 3.8, will be presented.
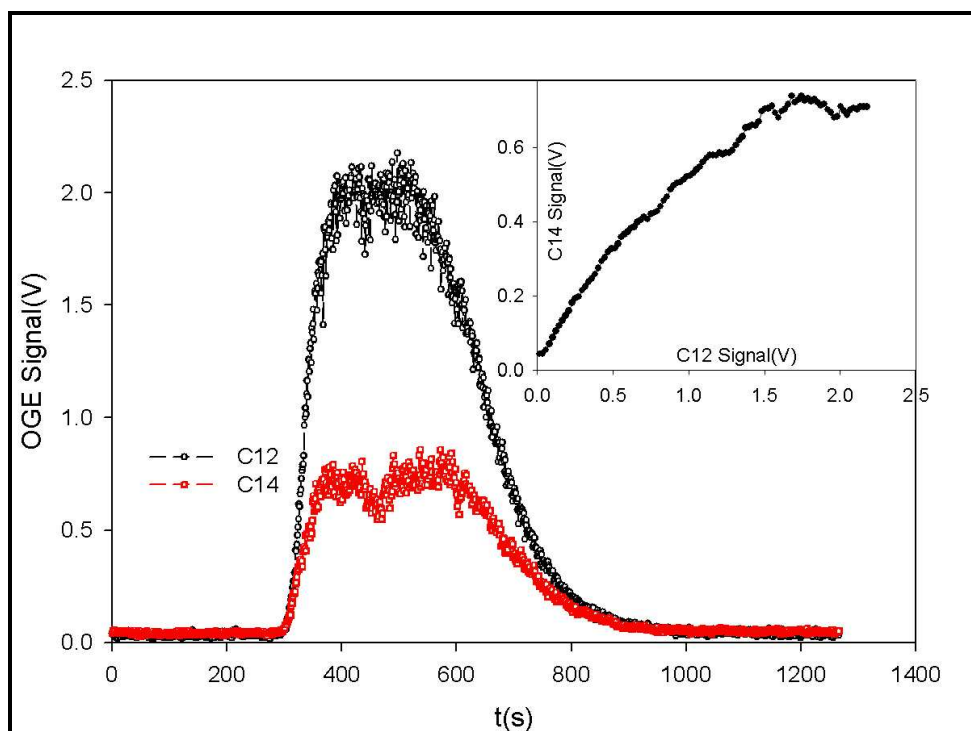
Figure 3.8 The buildup and loss of 1 ml of pure CO_2 sample with natural levels of radiocarbon injected onto a stream of CO2-free carrier gas flowing at 1 sccm. The cell pressure was kept constant at 5 Torr throughout the experiment.

Flow mode operation has the advantage of eliminating the memory effect and increased sample throughput, however it does not allow long term time averaging as in the case of batch mode analysis.

3.6.1.3 Sample Preparation

Calibration samples in the form of pure CO_2 with various ^{14}C enrichments were prepared for us at the Lawrence Livermore National Labs' AMS facilities in Livermore, California. They were delivered in approximately 4 inches long and 1/4 or 3/8 inches O.D. breakseal pyrex vials. The vial is inserted in a ½ in. I.D. bubble tubing as shown in Figure 3.9. [61] A dry ice - isopropyl alcohol bath is placed under the vial so that possible

water vapor in the vial is condensed and prevented from getting into the analysis cell along with CO_2 gas. Next, the tip of the vial is broken and the gas is allowed to expand throughout the reservoir volume. Sample collection efficiency is increased by cryogenically trapping the sample with liquid nitrogen in a buffer section as shown in Figure 2. Depending on the sample introduction method, the gas samples were sent directly to the intracavity analysis cell form the reservoir or they were plunged out via the septum with a gas tight syringe and introduced on the flow of carrier gas as described above.
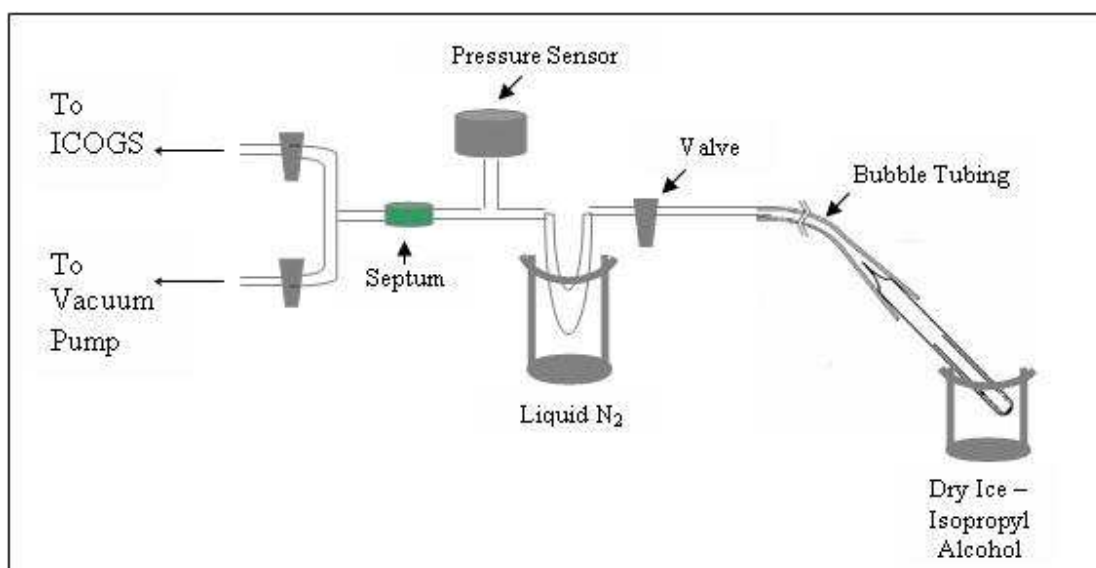
Figure 3.9 Schematic of sample preparation procedure

Chapter 4 :   Calibration Studies

4.1   Overview

The details of the experimental setup and the measurement procedures given in the previous chapter show that this new radiocarbon analyzer is a more compact and versatile instrument than AMS. The configuration may be varied depending on the application requirements. In this chapter, we will first give a detailed analysis of the background contribution to the measured optogalvanic signal from the more abundant carbon isotopes. Next, we will explain the signal enhancement mechanism via intracavity technique, pointing out analogies with the well studied ICAS method. In the last section, we will present the experimental results and system calibration with AMS measurements.

4.2   Lineshape Analysis

One of the most important characteristics of an absorbing or emitting medium such as the glow discharge in our experiment is its spectral line profile, which is broadened around a central resonant frequency due to intermolecular collisions as well as the thermal motion of molecules. Collisional interactions of the molecules increase the decay rate from the excited state, thereby leading to a homogenously broadened lineshape given by a Lorentzian distribution (Figure 4.1) [66, 67]:

$$S(v) = \frac{(1/\pi)\delta v_0}{(v - v_0)^2 + \delta v_0^{\,2}}$$

where δv_0 is the half width at half maximum (HWHM) of this function which is proportional to the collision rate:

$$\delta v_0 = \text{collision rate} \,/\, 2\pi$$

The collision rate is determined by the relation;

$$\frac{1}{\tau} = N\sigma\bar{v}_{rel}$$

Here, N is the number density of molecules, σ is the collision cross section and $\bar{v}$ is the average relative velocity of the molecules given by;

$$\bar{v}_{rel} = \left[\frac{8RT}{\pi} \left(\frac{1}{M_X} + \frac{1}{M_y} \right) \right]^{1/2}$$

where R is the universal gas constant and M is the molecular weight of the colliding molecules. The relation for collision rate implies that the main source of collisional broadening is the pressure of the gas medium. For our experimental system, the discharge cell contains 5% CO_2 in Nitrogen or 100% CO_2 with a total pressure of 1 to 5 Torr. Gas temperature is determined by measuring the difference in cell pressure before and after the discharge is initiated. In a brief trial, cell pressure increased from 1.213 Torr to 1.466 Torr which implies 21% change and using ideal gas law, final gas temperature is calculated as 310 K. The collision cross sections between CO_2-CO_2 and CO_2-N_2 are 1.57 x 10^{-18} m^2 and 1.2 x 10^{-18} m^2, respectively [68]. Using these values, FWHM of the collision broadened line shape is found to be about 38.4 MHz for 5% CO_2 in N_2 and 9.7 MHz for 100% CO_2.

In addition to collisional broadening, the lineshape is also broadened inhomogenously due to the Doppler effect which arises from the fact that each molecule in the discharge may experience a small shift in resonance frequency due to having different velocity component along the axis of radiation. Effective resonance frequencies are therefore distributed across the line center of a Gaussian distribution (Figure 4.1) given by:

$$S(\nu) = \frac{1}{\delta\nu_D}\left(\frac{4\ln 2}{\pi}\right)^{1/2} e^{-4(\nu-\nu_0)^2 \ln 2/\delta\nu_D}$$

where $\nu - \nu_0$ represents the shift from the line center frequency ν_0 and $\delta\nu_D$ is the full width at half maximum (FWHM) of the absorption curve given by:

$$\delta\nu_D = 2\frac{\nu_0}{c}\left(\frac{2kT}{m}\ln 2\right)^{1/2}$$

Here, m is mass of the $^{14}CO_2$ molecule in kilograms and T is the discharge temperature expressed in Kelvins. Taking the frequency of the $^{14}CO_2$ line center at P(20) as 25.476 THz [49], FWHM of the Doppler broadened line width at 310 K is calculated to be about 47.3 MHz.

In such cases where both the intermolecular collisions and the Doppler effect play a role in the broadening of the spectral line, the line shape function is given by the Voigt profile which is a convolution of the Gaussian and Lorentzian distributions (Figure 4.1). The line intensity is given by;

$$S(\nu) = \frac{0.939}{\delta\nu_D}\operatorname{Re} w(x+ib) \tag{1}$$

where, w is an error function of a complex argument. The parameters of this function are:

$$x = 1.67\frac{(\nu_0 - \nu)}{\delta\nu_D}, \quad \text{and} \quad b = 1.67\frac{\delta\nu_0}{\delta\nu_D}$$

whose values are tabulated in references [69]. Figure 4.1 shows the numerically computed Voigt profile superimposed onto Doppler and Lorentzian broadened line shapes with equal line widths [70]

$$x = (\nu - \nu_0)/2\delta_D$$
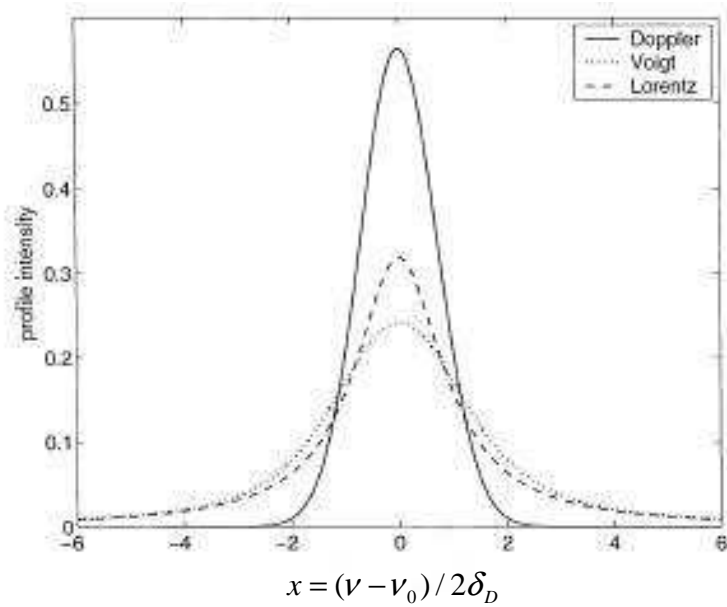
Figure 4.1: Voigt profile (dotted line) corresponding to Lorentz profile (dashed line) with half width equal to that of Doppler (solid line) half width $\delta\nu_D = 1$

Figure 4.2 shows resonance curves obtained by tuning the laser across its gain profile by ramping the PZT as explained in the previous chapter. In the first scan (Figure 4.2) the analyte cell contains pure nitrogen gas at 5 Torr, and it verifies that the cell is void of any molecule in resonance with $^{14}CO_2$ laser. For the second scan, the cell is filled with 5% CO_2 in Nitrogen that has 10 Modern radiocarbon. As shown in the Figure 4.3, the PZT scan yielded the optogalvanic effect line shape that shows the Voigt profile with a FWHM of about 50 MHz.
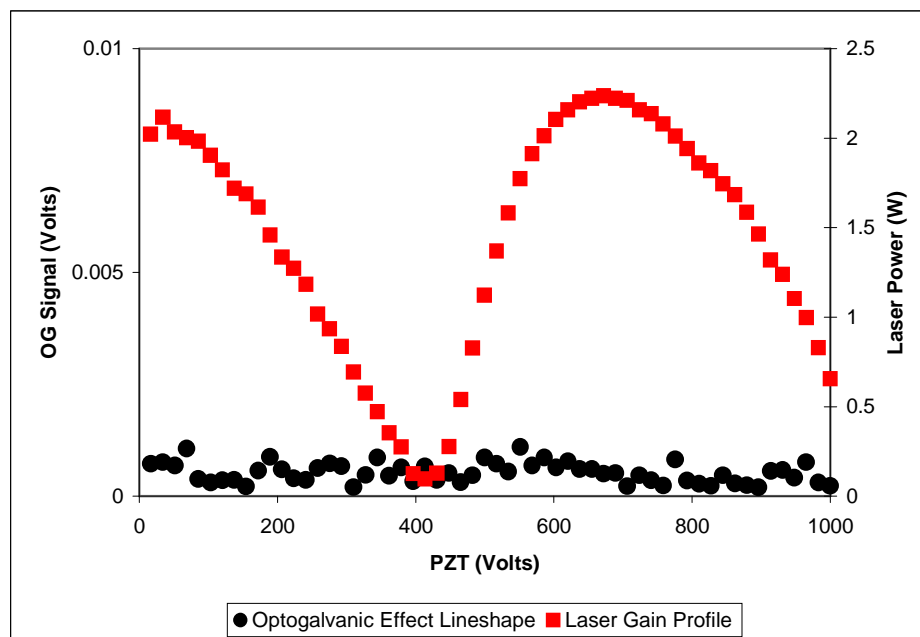
Figure 4.2 No resonant OGS when cell is filled with pure N_2, as expected.
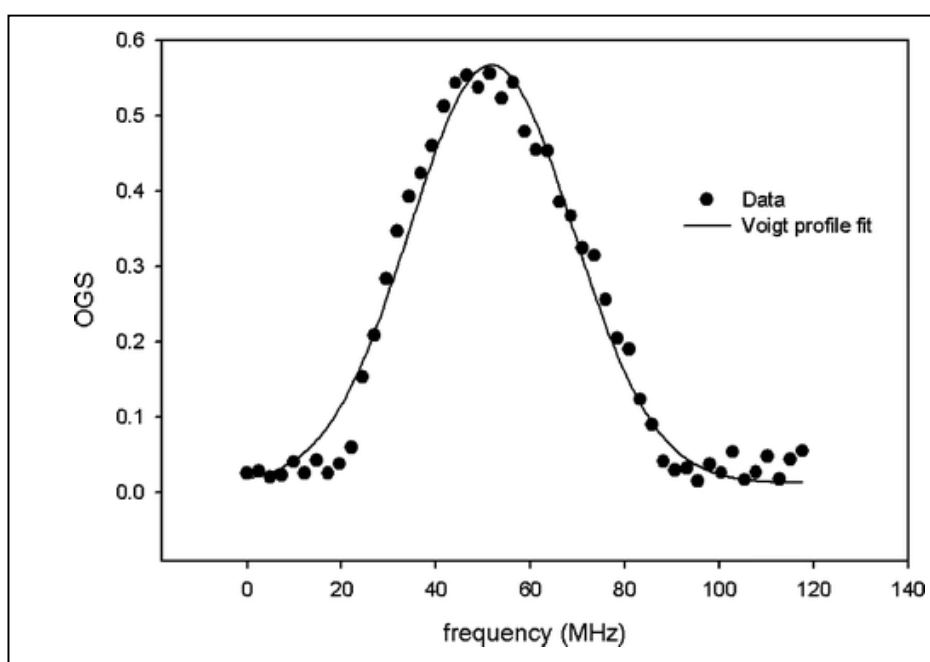
Figure 4.3 Resonance curve for intracavity optogalvanic effect when the cell is filled with 5% CO_2 in Nitrogen. The solid line is a best-fit Voigt profile with FWHM of about 50 MHz, as expected for $^{14}CO_2$ in the 5 mbar discharge at 310 K

The lineshape analysis is also critical in determining the background contribution to the optogalvanic signal from more abundant isotopes namely $^{12}CO_2$ and $^{13}CO_2$. As mentioned in earlier chapters, strongest emission lines of CO_2 lasers correspond to transitions between rotational quantum number $J = 19$ of the first excited vibrational level of the asymmetric stretch mode (00^01) and $J = 20$ of the first excited vibrational level of the symmetric stretch mode which is denoted by P(20) line. This follows from the Boltzmann distribution of rotational level population densities for a system of molecules in thermal equilibrium at temperature T, that is defined by the relation;

$$N_J(\nu) \propto (2J+1)\exp(\frac{-hcBJ(J+1)}{kT})$$ (2)

where B is the rotational constant of the molecule, which is inversely proportional to the moment of inertia I of the molecule and given by $B = (\frac{h}{8\pi^2 cI})$.

The resonant line center frequency for $^{14}CO_2$ P(20) line is at 25.476 THz. Although the nearest $^{12}CO_2$ and $^{13}CO_2$ lines are separated by more than 400 line widths (Figure 4.4), due to more than 10 orders of magnitude difference in natural isotopic abundance there exists a non-resonant background contribution to the total OGE response. In order to determine the line intensity from $^{12}CO_2$ and $^{13}CO_2$, we picked the six closest $^{13}CO_2$ lasing transitions, and one $^{12}CO_2$ transition to this frequency from the tabulated values [49], namely P(68), P(66), P(64), P(70), P(72), P(74) of $^{13}CO_2$ and P(82) of $^{12}CO_2$.
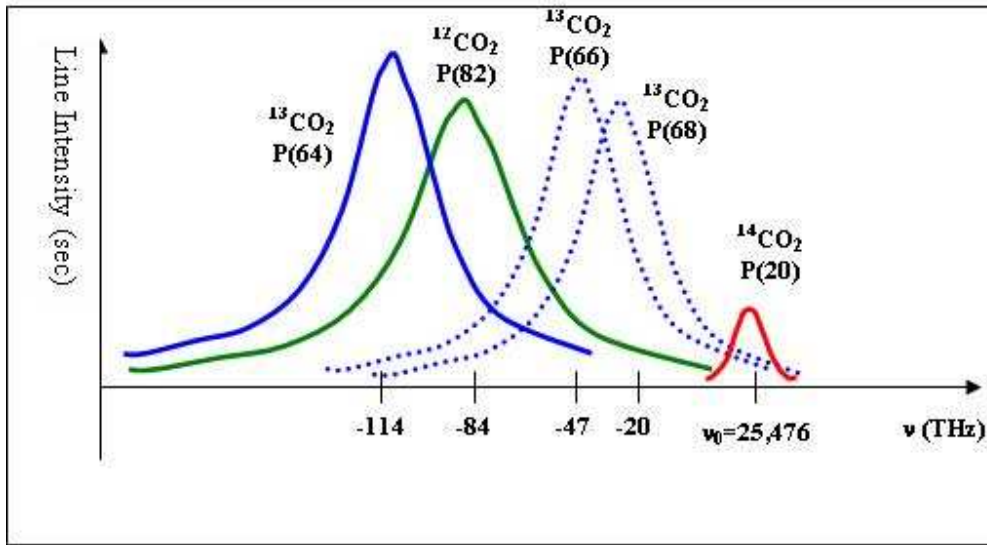
Figure 4.4 Relative distance of line centers of more abundant isotopes from the resonant line center of $^{14}CO_2$. Background contributions to the signal from 4 of these lines is pictured as example

Next, the intensity of the Voigt profile at the line center for $^{14}CO_2$ is calculated using Eq. (1) together with the tabulated values for Voigt parameters [70]. After that, we used the Lorentzian distribution to calculate the far wing limits of these 7 lasing transitions, since the intensity of the Doppler profile outside of its FWHM approaches to zero much sooner than the Voigt profile due to the exponential decay. We also calculated the ratio of the rotational level populations using Eq (2) and finally multiplied the intensity of the profiles to correct for the difference in natural isotopic abundances, i.e. 10^{12} times for $^{12}CO_2$ and 10^{10} times for $^{13}CO_2$. Following a similar approach, we calculated the total contributions to the signal at a lower pressure, as well as the case when R(20) line of $^{14}CO_2$ could be chosen as $^{14}CO_2$ laser emission.

Table 4.1 summarizes the results of the calculations and shows the partial contribution to the line strength from each isotope compared to 1 Modern $^{14}CO_2$ which is also a measure

of the total OGS. For higher values of $^{14}CO_2$, the ^{14}C contribution in the signal increases whereas the ^{12}C and ^{13}C remains constant.

5 Torr			1.1 Torr		
C12	**C13**	**C14**	**C12**	**C13**	**C14**
R(20): 250 :	1667 :	1	R(20): 60 :	400 :	1
P(20): 11 :	1 :	1	P(20): 0.2 :	3.2 :	1

Table 4.1 Contributions to the OGS from most abundant carbon isotopes calculated for a pure CO_2 sample with 1 Modern ^{14}C (i.e. isotopic ratios of $^{14}C/^{12}C \sim 10^{-12}$ and $^{14}C/^{13}C \sim 10^{-10}$) R(20) and P(20) correspond to the two $^{14}CO_2$ laser emission lines with the highest gains.

As seen from the results, optogalvanic signals collected using the laser emission from the R(20) line of $^{14}CO_2$ laser would be made up of mostly ^{12}C and ^{13}C background signals. When the laser is tuned to P(20) line, percentage of resonant $^{14}CO_2$ signals gets bigger and especially at lower pressure, around 23% of the OGS is expected to be from resonant laser interaction specifically with $^{14}CO_2$ molecules. In light of this calculation, experiments for system calibration are done by using P(20) line of $^{14}CO_2$ and keeping the cell pressure around 1 Torr. Although in principle lowering the pressure beyond 1 Torr would bring the background even lower, this also results in higher noise and smaller signal amplitude.

4.3   Signal Enhancement via Intracavity Detection Technique

Cavity-enhanced spectroscopic methods, such as Intracavity Absorption Spectroscopy (ICAS), provide a remarkable improvement in signal detection sensitivity over conventional absorption spectroscopy especially for analyzing gas samples. As shown in

Equation 1.1, the recorded signal in absorption studies is the transmitted laser intensity through an absorbing medium with path length L with absorber density n. The product of the absorption cross section and the absorber density is called the absorption coefficient κ, where $\kappa = n\sigma(\upsilon)$. In general, the detection limit in absorption spectroscopy is defined as the smallest detectable absorption coefficient, κ_{min}. The minimum absorption coefficient detected using ICAS is of the order of 10^{-10} cm^{-1} which is about 10^9 times greater than that of the conventional absorption measurement technique and implies a detection sensitivity of the order of part per billion in absorber concentration. [28, 30, 71, 72] In addition, from Equation 1.2, it can be understood that the highest detection sensitivity can be achieved by improved signal to noise ratio in the recorded signal and also by increasing the absorption path length. In ICAS, the ratio of absorbance signal to absorption coefficient gives the effective absorption path length L_{eff} and it is used as a measure of the spectral sensitivity of the system. Here, effective path length corresponds to the distance that incident light would travel to produce an equivalent signal in a conventional, single pass absorption experiment. Since the Optogalvanic Signal is also proportional to laser interaction length as shown in Eq 2.8, it will be valuable to study the physical mechanisms leading to enhanced spectral sensitivity in ICAS.

Firstly, the intensity inside the laser is larger by a factor of $q = 1/(1 - R_1 R_2)$ than the outside of the laser where R_1 and R_2 are the reflectivities of the back mirror and the output coupler of the laser. This provides an advantage similar to that of a multipass cell inside a resonator.

In addition, contrary to ICOGS, highest sensitivity with ICAS has been demonstrated by using broad-band multimode lasers operating close to its lasing threshold and an

intracavity absorber whose linewidth is smaller than that of the laser medium. Since the output power of the laser depends on the gain of the laser medium and the losses inside the resonator, as the laser is tuned across its gain profile, certain dips in the laser emission profile are observed, as seen in Figure 4.5. These relative intensity changes are then analyzed to determine trace levels of atomic and molecular concentrations.
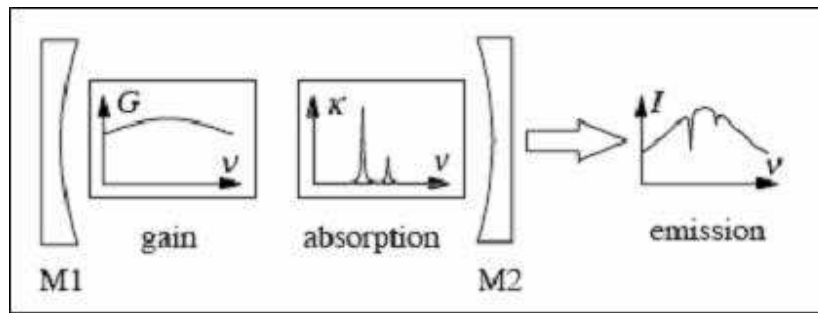
Figure 4.5 ICAS measurement schematics from[28]. Laser cavity is formed by totally reflecting back mirror M1 and partially reflecting output coupler M2. The laser cavity includes an absorptive medium with a narrower line width than that of the laser's gain medium.

This effect is greatly enhanced when the laser is operating close to threshold, which can be explained in the following way: During the steady state operation of the laser, saturated gain of the laser equals to the total losses of the cavity, such that

$$g_s = \frac{g_0}{1 + I/I_s} = l$$

where g_s is the saturated gain of the laser, g_0 is the small signal gain and I_s is the saturation intensity of the laser. If we solve for the laser emission intensity;

$$I = I_s \frac{g_0 - l}{l}$$

When additional small losses are introduced by placing an intracavity absorber, change in the laser intensity is given by,

$$dI = -I_s \frac{g_0}{l^2} dl$$

Then the relative change in intensity is;

$$\frac{dI}{I} = -\left[\frac{n}{l(n-1)} \right]$$

where $n = g_0/l$. Comparing the case where the same absorber is placed outside the laser cavity, in which small changes in the intensity would equal to small losses by the absorption cell, an enhancement factor Q can be defined as:

$$Q = \frac{g_0}{l(g_0 - l)}$$

When the laser is close to its threshold, g_0 approaches to l therefore the enhancement becomes very large. However, laser instabilities close to threshold reduce the signal to noise ratio and this puts an upper limit to the sensitivity that can be achieved experimentally.

As mentioned earlier, highest sensitivity with ICAS technique is achieved with multimode lasers. As the laser intensity drops at certain frequencies that correspond to losses caused by the intracavity absorber, neighboring laser modes gain intensity in such a way that they compensate the losses and keep the laser operating above its threshold. This mode competition may cause even further decrease in the intensity of the absorbed line. So, even the smallest intracavity absorption may lead to big changes in the laser intensity at that resonant mode. The existence of a finite time for development of a laser mode dictates an upper limit to the measurement time t, such that $0 < t \leq t_{mode}$. Typical mode lifetimes in cw laser systems can vary from 10 μsec to milliseconds [72]. The

maximum spectral sensitivity that can be achieved with this technique can be expressed in terms of an effective path length, given by,

$$L_{eff} = ct$$

where c is the velocity of light and t is the measurement time. The highest sensitivity achieved with a cw multimode laser corresponds to an effective absorption path length of 7×10^7 meters.

There are several studies that focus on the limiting conditions of the enhancement in sensitivity with ICAS using cw multimode lasers from both theoretical and experimental perspectives [28, 72, 75]. Especially the work of Atmanspacher et al demonstrated the saturation effects caused by increased measurement time as well as spectral power density as shown in Figure 4.6.
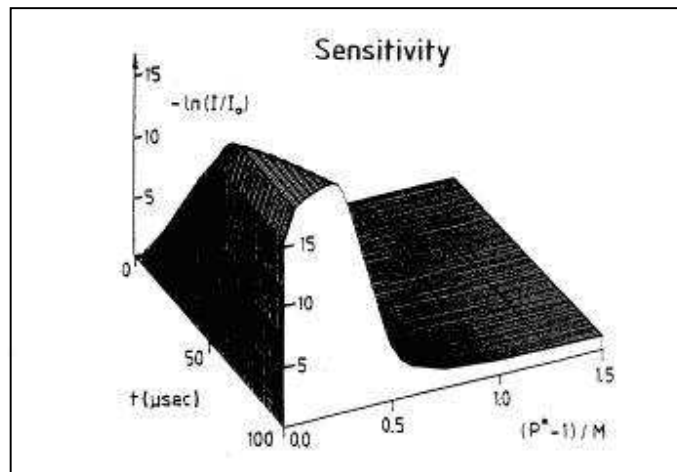
Figure 4.6 Quantitative model of Intracavity Absorption show the saturation of absorption signal and hence the sensitivity with increasing measurement time and laser power. (From reference [72]) For this calculation, 589.0 nm Na D2 resonance line with an assumed line width of 3 GHz and an absorber concentration of 10^9 cm^{-3} was used

In the figure above, absorption signal and hence the sensitivity, given by $-\ln(I//I_0)$, is highest at low pumping powers, i.e. when the laser is operating close to threshold and

also at longer measurement times. Here $P^* = P/P_{thr}$ and M is the number of oscillating

laser modes. Saturation effects are also apparent at longer observation times and higher

laser powers before the signal turns over at sufficiently high powers above laser

threshold.

In addition to saturation effects due to laser power and measurement time, Baev et al [28]

predicted non-linearity of enhancement in sensitivity with increasing absorber density for

ICAS using single-mode lasers when they operate close to threshold. By solving the rate

equations for laser photon number and population of upper laser level for various

absorption coefficients, authors demonstrated that sensitivity enhancement decreases

non-linearly with increasing absorber concentration, as shown in Figure 4.7.
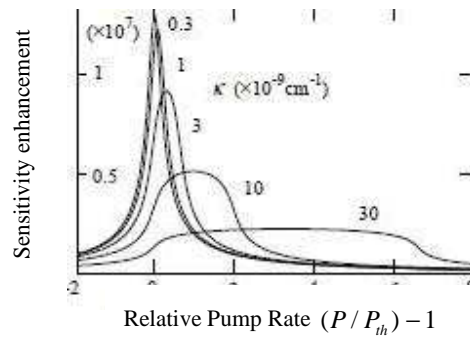
Figure 4.7 Biggest enhancement in sensitivity is achieved at pump rates close to laser threshold. Under same operating conditions, sensitivity enhancement decreases non-linearly with increasing concentration (n) indicated by the absorption coefficient κ=nσ(ν). [28]

In summary, effective path length, L_{eff}, which is a measure of spectral sensitivity of the

measurement system, depends on saturation effects due to laser power and measurement

time and also the sample concentration. In the upcoming sections, we will present the

results of experiments carried out with the new radiocarbon detection system. We will

elaborate on similarities with the ICAS technique in terms of enhancement in detection sensitivity as well as the observed saturation effects.

4.4 System Calibration

As mentioned earlier, this work is aimed at developing a new instrument suitable for routine laboratory use for quantitation of radiocarbon in biomedical samples around Modern enrichments as well as carbon dating of small samples. The instrument will have orders of magnitude greater sensitivity than scintillation counters and will be able to replace AMS for several applications.

The measurement capabilities of this new technique is now demonstrated with calibration intervals of over more than three orders of magnitude using pure CO_2 gas at a pressure around 1.1 Torr and laser modulation frequency of 17 Hz. Due to observed laser saturation effects, two different calibration curves are obtained. Figure 4.8 shows the calibration from 10^{-3} Modern to 0.97 Modern and Figure 4.9 shows calibration from 0.11 Modern to 12 Modern samples with the OG signals plotted against AMS results. Measurements with 100 Modern sample yielded signals with lower amplitude than that of 12 Modern.

These results show that we have obtained an enhancement of about 10^7 with the intracavity configuration compared to a single pass system. We have demonstrated a limit of detection to isotopic ratios of the order of 10^{-15} which is similar to AMS. Only a few thousand $^{14}CO_2$ molecules can be detected with great sensitivity using less than micrograms of pure CO_2 sample.
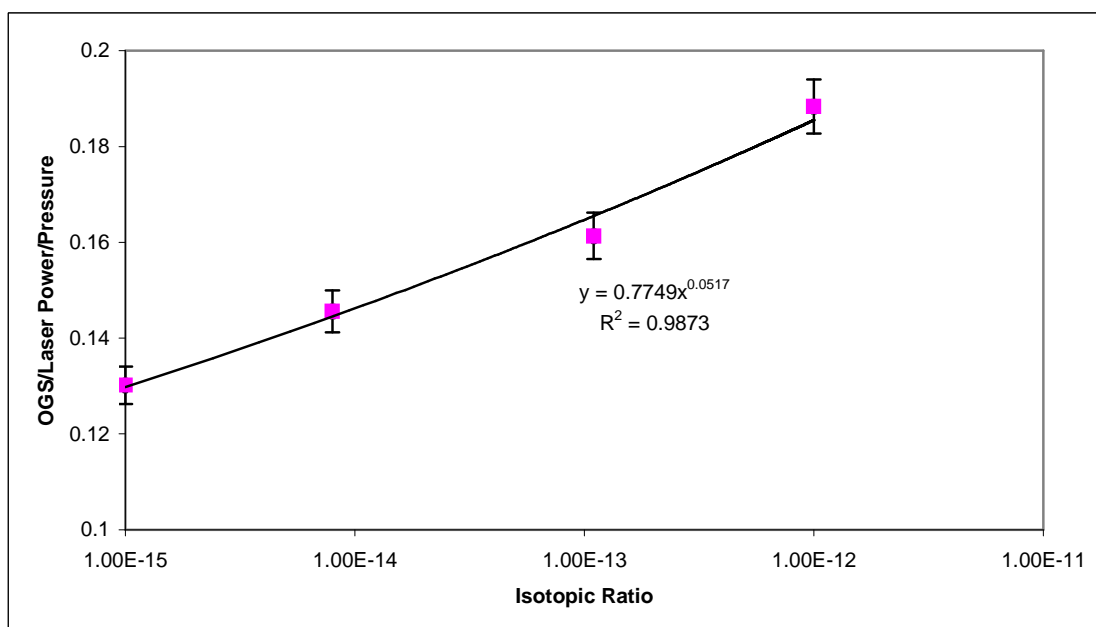
Figure 4.8 Calibration curves obtained with Optogalvanic signals plotted against AMS results. For ^{14}C concentrations less than 1 Modern, analysis was carried out with high laser power to achieve highest sensitivity
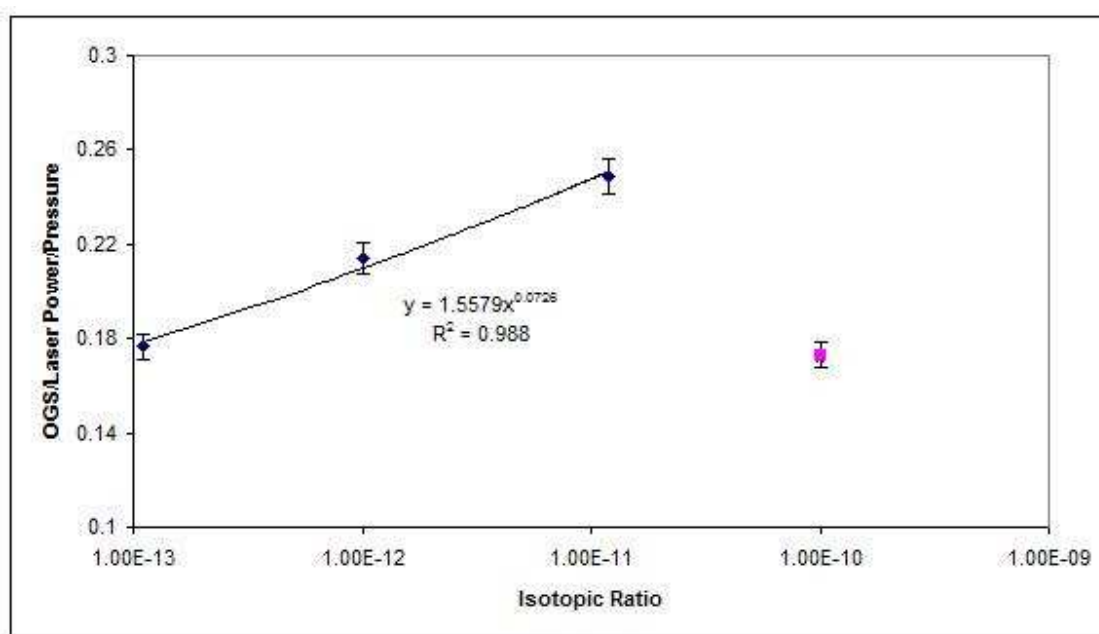
Figure 4.9 For ^{14}C concentrations greater than 0.11 Modern, analysis was carried out with lower laser power

These two calibration curves are obtained with measurements carried out in batch mode as outlined in the previous chapter. Briefly, after filling the cell with pure CO_2 sample to about 1.1 Torr, the glow discharge is turned on and given about a minute to stabilize. Next, the data acquisition program is run to perform a PZT scan across the laser gain curve and variation in the optogalvanic signal is recorded as shown in Figure 4.10.
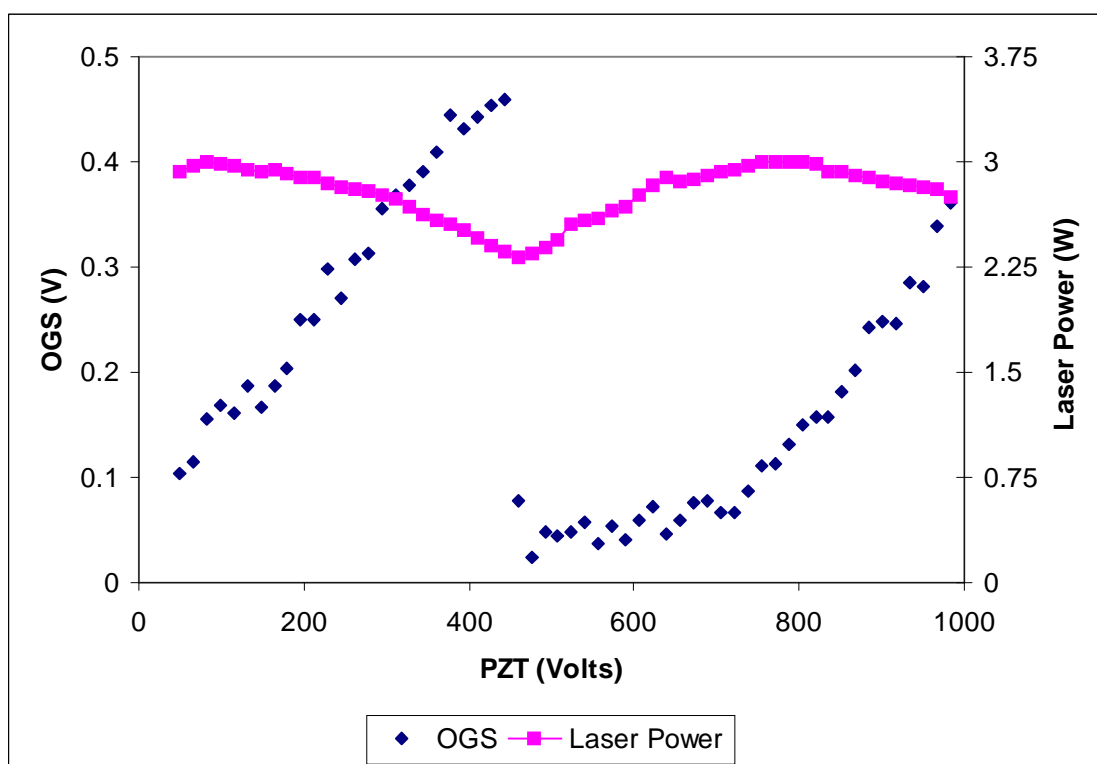
Figure 4.10 Change in the optogalvanic signal (left y-axis) is measured from the variation in the gain of the laser (right y-axis). Analyte is pure CO_2 gas with 0.11 Modern radiocarbon.

This scan is repeated for 3 different laser powers which is adjusted by manually by changing the laser discharge current via the laser exciter. For samples with low ^{14}C concentrations (<1 Modern) measurements are done with high laser power, whereas for samples with high concentrations (>1 Modern) lower power values are used for

normalization. The ratio of OG signal per laser power is then normalized to the gas pressure. The sample consisted of pure CO_2 gas, so pressure normalization gives a measure of the radiocarbon ratio to more abundant isotopes. It has been verified experimentally that the optogalvanic signal changes linearly with pressure (Figure 4.11). This final normalized value corresponds to the isotopic ratio indicated on the calibration curves above.
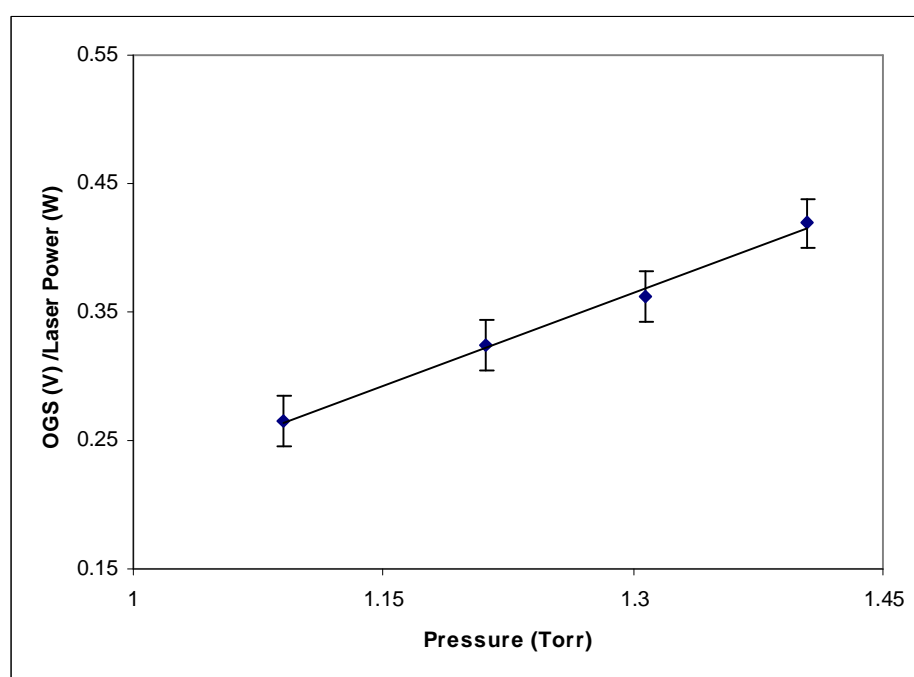
Figure 4.11 Optogalvanic signal changes linearly with pressure.

System calibration studies were also carried out in flow mode measurement procedure. For this purpose, initial experiments were done to determine how the signal amplitude changes with flow rate. As shown in the figure below (Figure 4.12), $^{14}CO_2$ optogalvanic signal amplitude increases with increasing flow rate. At each step of increase in flow, the RF power sustaining the discharge was tuned to obtain the minimum noise possible. However, the background noise is also observed to increase with increasing flow rate.

Therefore, for calibration purposes, we have chose to operate around 0.05 ml/min flow rate which yield relatively higher signal to noise ratio.
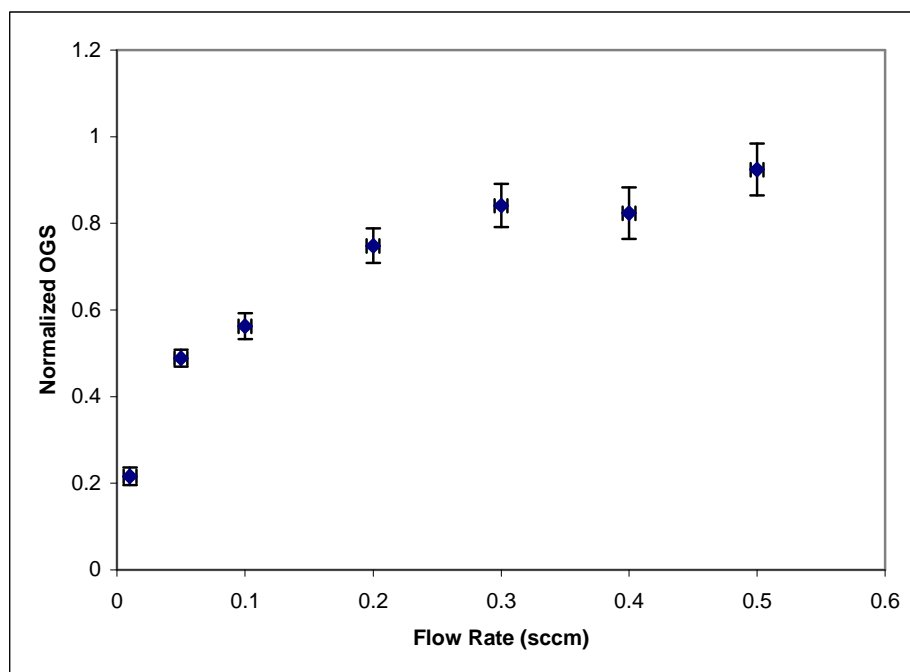
Figure 4.12 Optogalvanic signal increases non-linearly with increasing flow rate.

Calibration measurements of samples with different ^{14}C concentrations were carried out in a similar way to that of batch mode analysis. Following a PZT scan at varying laser power values, the peak signal is plotted against laser power to see the laser power saturation effects and determine the optimum operating power that would yield a linear calibration curve. (Figure 4.13)
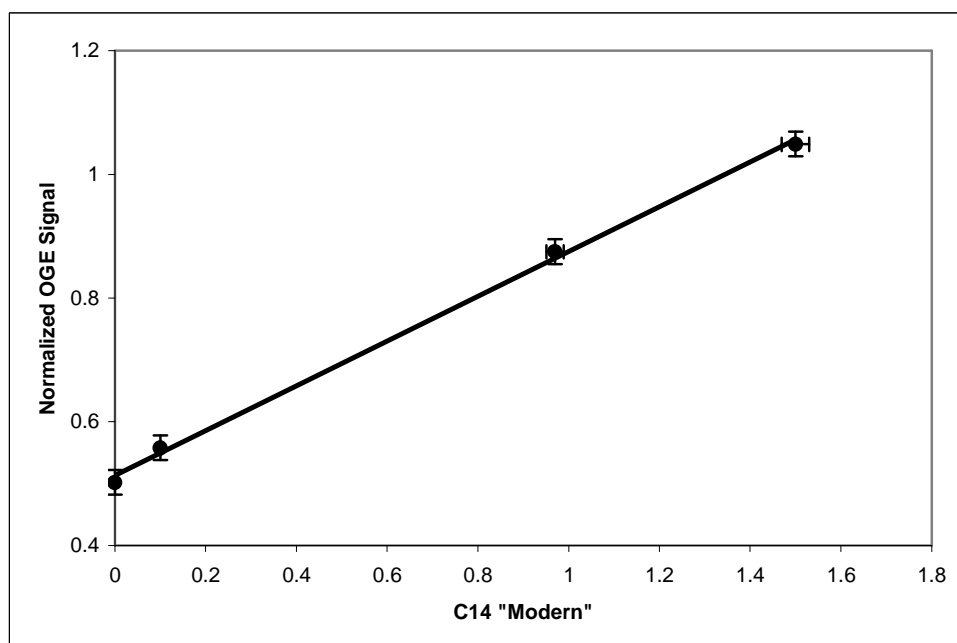
Figure 4.13 Linear calibration curve obtained in flow mode measurements. Pure CO_2 sample flow rate is 0.05 sccm, the laser is modulated at 17 Hz and the signals are normalized to laser's OGE output

As shown in the graph above, optogalvanic signal changes linearly with ^{14}C concentration variation over more than 1 order of magnitude. A 12 Modern sample yielded a lower normalized signal of 0.686 V/W, an effect that was also observed in batch mode calibration measurements. However, in the batch mode measurement, turning over of the signal happened at a higher concentration than 12 Modern.

These results indicate the huge sensitivity obtained via the new Intracavity Optogalvanic Spectroscopy technique. Linearity and the dynamic range of the calibration curves depend on laser power, laser modulation frequency and resonant molecule concentration. The effects of these parameters on the optogalvanic signal will be studied in more detail in the following sections, emphasizing similarities and differences with ICAS.

Chapter 5 : Dynamics Of Intracavity Optogalvanic

Spectroscopy

5.1   Overview

The calibration curves presented in the previous chapter (Figure 4.8 and 4.9) show the huge enhancement in sensitivity achieved with this new laser based radiocarbon detection method. The dynamic range of these calibration intervals imply that with this technique quantitation of ^{14}C in biochemicals as well as trace levels of depleted radiocarbon in environmental samples can be done routinely with much less complexity than Accelerator Mass Spectrometry. Throughout the calibration studies Intracavity Optogalvanic Signal showed saturation effects with increased laser power and laser modulation frequency. In addition, for samples with high enrichments (>10 Modern), the calibration curve became non-monotonic. In this chapter, these non-linear effects will be studied in greater detail and also the operating procedures developed for measuring samples with unknown ^{14}C content will be presented.

5.2   Signal Dependence on Laser Modulation Frequency and Laser Power

The optimum calibration interval for isotopic ratios less than or equal to 1 Modern is obtained by utilizing maximum laser power (~50 W internal) whereas the best fit for higher enrichments (1-12 Modern) was obtained for measurements done with lower power (~ 25 Watt) to avoid laser power saturation effects. However, under the same operating conditions, i.e. same laser power and laser modulation frequency, 100 Modern

sample yielded lower signal amplitude as seen in Figure 4.9. Even though our goal was to obtain highest sensitivity possible with this new intracavity technique, this effect showed the non-linearity in signal enhancement when the concentration is varied over more than 5 orders of magnitude. As mentioned in the previous chapter, effective path length L_{eff} and intracavity laser intensity characterize the enhancement in signal sensitivity. So we study these parameters in further detail to better understand the dynamics of ICOGS.

Figure 5.1 shows a typical optogalvanic signal waveform as a response to a periodically modulated laser beam incident onto the glow discharge consisting of 5% 0.97 Modern CO_2 sample in Nitrogen. In previous external cell measurements for stable isotope ratio analysis of CO_2, highest SNR values were obtained around 5% CO_2 in Nitrogen. [41, 43] In Chapter 2, it was mentioned that having Nitrogen in the analysis cell, enhanced the OG signal for the same reason a CO_2 laser output is increased by efficient energy transfer between electronically excited nitrogen molecules and upper laser level of CO_2. In this case, the discharge can be viewed as a gain system and upper laser level population is depleted due to stimulated emission, therefore loss of energy to the incoming laser field leads to cooling of the gas. This local temperature decrease leads to an increase in particle number density, a decrease in electron mobility and thereby an increase in impedance of the discharge [76]. The averaged waveform in Figure 5.1 shows the increase and decrease in optogalvanic signal due to laser radiation going ON and OFF which is indicated by the 0-5 Volt chopping signal.
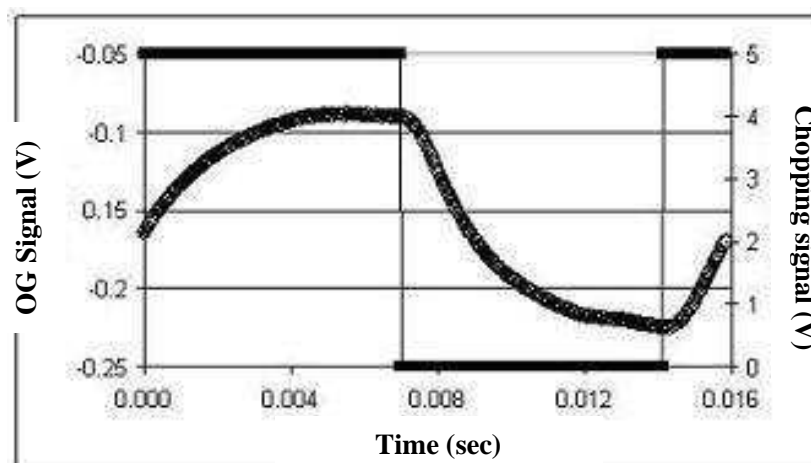
Figure 5.1 Typical OG Signal in response to a laser modulated at 63 Hz. Laser ON-OFF time indicated by 0 to 5 V TTL trigger pulse. 5 sec averaged signal measured for sample of CO_2 gas with 0.97 Modern enrichment in Nitrogen.

On the other hand, if the discharge system is in absorptive condition, an opposite effect, namely heating effect of the gas leads to an optogalvanic signal with an opposite sign as shown in Figure 5.2. In this case the discharge consists of pure CO_2 gas and the irradiation of the discharge with the resonant beam causes an overall heating of the gas which leads to a decrease in the discharge impedance.
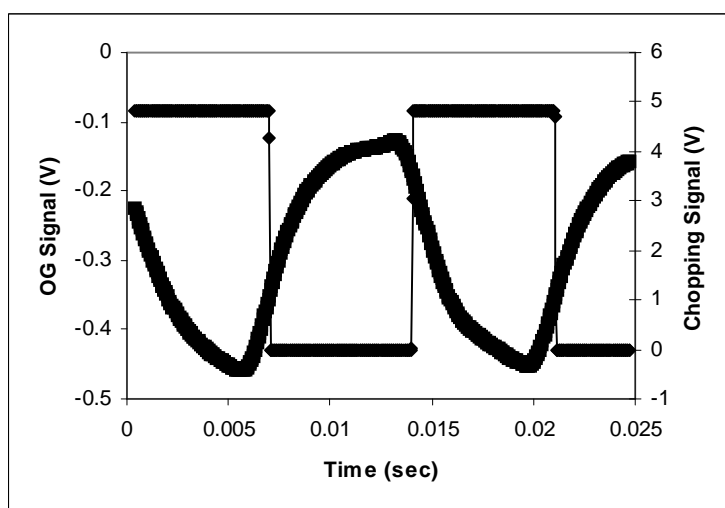
Figure 5.2 OG Signal measured for pure CO_2 gas at 1.1 Torr with 0.97 Modern enrichment and the laser modulated at 71 Hz

As mentioned in Chapter 2, Smith and Moffatt [47] gave a temperature model of the OG effect which is in good agreement with many measurements [51,52]. They have shown that the fractional change in a DC-excited laser discharge power is directly proportional to the fractional change in molecule number density brought about by laser irradiation. Also, from the ideal gas law, this ratio is proportional to the change in gas temperature. That is;

$$\frac{\Delta P}{P} = \frac{\Delta n}{n} = -\frac{\Delta T}{T} \tag{5.1}$$

The discharge power is given by relation $P = I.V$ and at constant current, $\Delta P = I.\Delta V$, where ΔV is the voltage change in the cell. Therefore, Eq. 2.7 can be written as;

$$\frac{\Delta V}{V} = -\frac{\Delta T}{T} \tag{5.2}$$

Although our system is an rf glow discharge, the same model should approximately hold. As seen in Figure 5.2, we measure an OG signal of about 0.3 Volts for ~1 Modern sample. So for our system, with a 2000 gain amplifier and 800 Volts rf driving voltage, we have $\frac{\Delta V}{V} = 1.87 \times 10^{-7}$. We can estimate the fractional change in gas temperature due to laser perturbation, as follows:

At 1.1 Torr gas pressure at 310 K and a concentration of 1 Modern, there are about 315,000 $^{14}CO_2$ molecules in the entire cell volume of 9.2 ml. In thermal equilibrium, the Boltzmann factor, given by;

$$Nj \propto (2J+1)e^{-\Delta E/kT} \tag{5.3}$$

implies ~39,000 $^{14}CO_2$ molecules in the lower laser level. Here, $J = 20$ and $\Delta E \cong 0.15\,eV$ is the energy of the lower laser level. I have determined ΔE from the tabulated value for

the frequency of the symmetric stretch mode for the $^{12}CO_2$ (1388 cm^{-1}) and using the fact that it is inversely proportional to the square root of the mass of the molecule, I have corrected this value for the higher mass of the $^{14}CO_2$ molecule. We have shown in Chapter 4 that more abundant isotopes, off resonance, are equivalent to ~ 3 times more $^{14}CO_2$ molecules at line center. So there are effectively 117,000 molecules in this state. The area of the laser beam is ~ 0.13 cm^2, whereas the cross section of the cell is 0.785 cm^2. So there are ~19,000 molecules in the irradiated part of the laser beam. For the experiment shown in Figure 5.2, laser output power was ~ 8 Watts, which imply ~ 98 W internal power due to 85% reflective output coupler and also taking the internal reflections into consideration. Since the energy of the resonant photon is ~ 0.105 eV, the standing wave laser cavity photon flux is 4.49×10^{22} photons.cm^{-2}.s^{-1}. Using the total absorption cross section of $\sigma = 7.9 \times 10^{-16}$ cm^2, which I calculated at the 11.768 μ resonant transition [66], the total energy gained by the discharge system in one laser irradiation period (~0.007 sec) due to absorption is $\sim 7.9 \times 10^{-11}$ Joules. From the kinetic theory of gases, we can determine the fractional temperature change ΔT, by using the relation;

$$E = \frac{3}{2} N_g k \Delta T \qquad (5.4)$$

where N_g is the total number of molecules ($\sim 3.15 \times 10^{17}$) and k is the Boltzmann constant. This yields $\Delta T = 1.2 \times 10^{-5}$ K, and $\frac{\Delta T}{T} = 3.9 \times 10^{-8}$.

This calculated temperature value is about 5 times less than that calculated from our measurements and equation 5.2. The difference is not unreasonable due to the approximate nature of the model and the fact that the ΔV measured is across a driving

transistor in a tuned RF oscillator circuit, not the ΔV across the discharge. A more detailed circuit and plasma analysis may yield more accurate estimate. In addition, all the parameters used in the calculation above, including the total number of absorbing molecules, the total absorption cross section and the photon flux, have uncertainties ~10%.

As seen in figure 5.2, it takes about 0.5 milliseconds to generate a measurable OG response, due to the fact that the optogalvanic response is a thermal effect caused by laser perturbation. Therefore the choice of laser modulation frequency should be below 2 kHz. In addition, as seen in the same figure, the OG signal rise time for the glow discharge to reach a new equilibrium condition is about 6 milliseconds. So, a choice of measurement time equal to or longer than the signal rise time is preferable. Although, longer measurement times, i.e. lower chopping frequency further decrease SNR by raising the 1/f noise, it is somewhat compensated by enhanced signal.

In light of these observations based on the optogalvanic signal waveform, further experiments were carried out to determine the time dependent characteristics of our measurement system. Figure 5.3 shows the variation of the optogalvanic signal for laser chopping periods from about 4 milliseconds to 60 milliseconds. In practice laser modulation frequency is varied between 17 Hz and 227 Hz. The graph includes two sets of data points for two different samples, namely 0.97 Modern which is of the order of contemporary levels of radiocarbon and "dead CO_2", that is the sample is obtained from fossil fuel combustion therefore it contains minimal ^{14}C but the stable isotopes ^{12}C and ^{13}C are present ($^{14}C/C \leq 10^{-15}$). The signals obtained from this dead CO_2 sample comes

from the more abundant isotope background effects that were explained in the previous chapter.
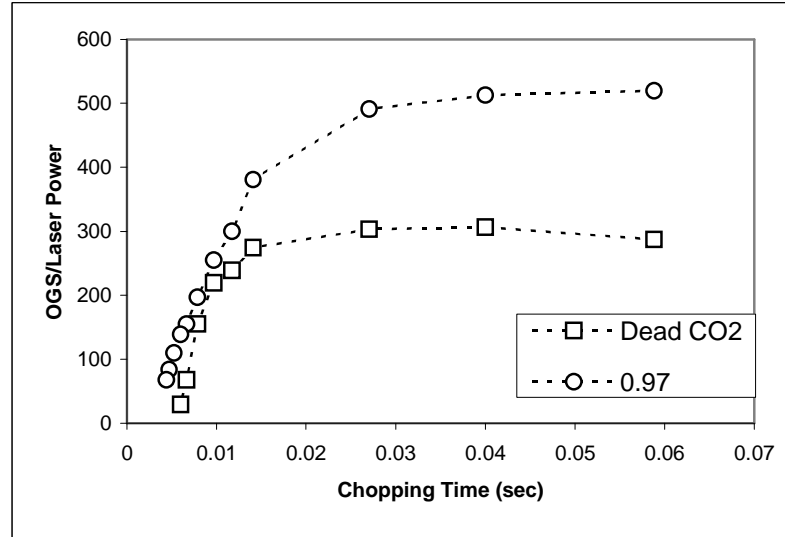
Figure 5.3 Experimental results show the measurement time dependence of normalized Optogalvanic Signal for two different samples. Experiments are carried out in the batch mode.

In the figure above, as the measurement time is increased, the spectral sensitivity, defined by effective path length ($L_{eff} = ct$), reaches a maximum value and levels off at different times for the two samples. Signal is enhanced for both ^{14}C and the background, however the enhancement clearly saturates for the non-resonant background signal at a shorter time than that of the resonant ^{14}C signal. In his thesis work with external cell optogalvanic signal measurements, Okil [43] has also shown that highest resonant $^{12}CO_2$ and $^{13}CO_2$ signals are obtained at a laser modulation frequency of about 25 Hz, that is 40 milliseconds, which is a similar result as seen in the figure above for the resonant $^{14}CO_2$ signal. But, in his experiments, he observed that the signal amplitude decrease was almost linear with decreasing chopping time. In our case, the signal enhancement introduced by

the intracavity configuration shows non-linear effects and saturates. For samples with 1 Modern or lower enrichment, longer measurement times yield highest SNR and hence the highest sensitivity. Even though the signal amplitude is lower at higher chopping frequencies, signals are still proportional to concentration and changes almost linearly for $t < 10$ milliseconds. Therefore, for higher enrichments, it is preferable to work at higher frequencies to lower the enhancement in sensitivity by lowering L_{eff} and possibly achieve a longer dynamic range.

In addition to laser modulation frequency, enhancement in sensitivity depend on laser intensity as well, implied by Eq 2.8. Figure 5.4 shows the relation between the OGS signal and laser power for the four calibration points on Figure 4.9. These experiments are carried out in batch mode procedure with pure CO_2 and 17 Hz laser modulation frequency. The laser power is varied by changing the laser pump power from the power supply between 225 Watt down to 55 Watt. For the 100 Modern sample ($^{14}C/C = 10^{-10}$) normalized signal amplitude is lower throughout. In addition to that, laser saturation effects are apparent at the highest pump power for this concentration value.
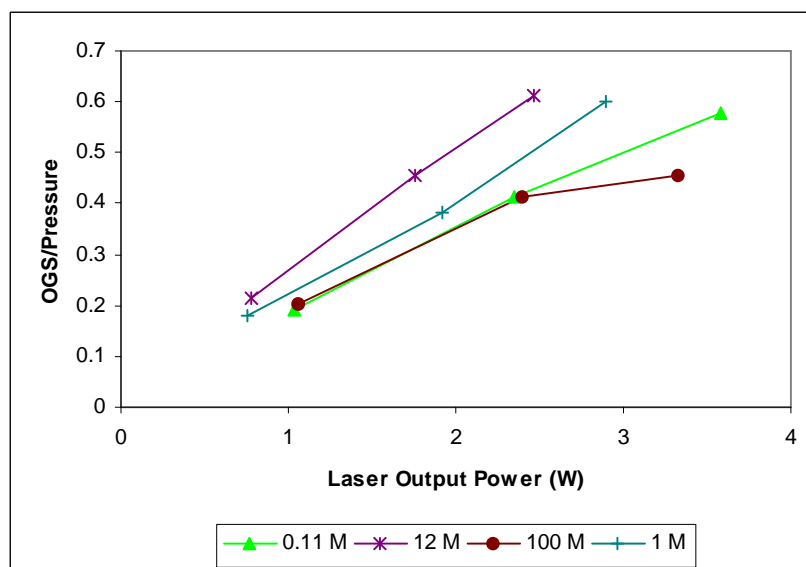
Figure 5.4 Normalized OGS vs Laser Power plot includes the effects of varying laser power on four ^{14}C values on calibration curve

In light of these observations, to test if we could get a calibration interval with larger dynamic range, short measurement time, i.e. high frequency and low pumping power experiments are carried out with 1, 12 and 100 Modern samples. The results are shown in Figure 5.5. Throughout these experiments, $^{14}CO_2$ laser is modulated at 227 Hz and laser's power supply was set to about 55 Watts which lead to 0.85 Watt laser output power. At high laser modulation frequencies, there existed a technical problem with the software program's phase locking algorithm in which case user had to manually adjust the mechanical chopper rotation speed to match the laser frequency to that of computer sampling frequency. Due to this effect, an estimated error of about 5% is indicated on the data points.
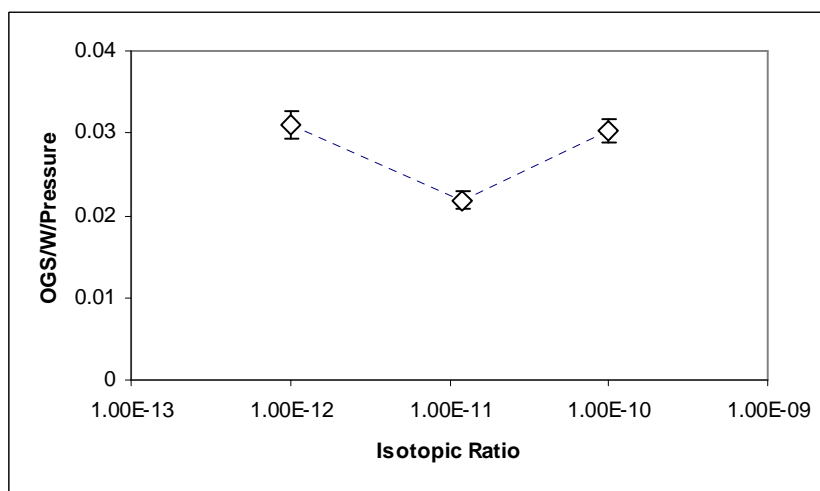
Figure 5.5 Calibration measurements with 227 Hz laser modulation frequency and 0.85 W output power show concentration dependence of signal enhancement.

As a result of high frequency, low power operation, we decreased the enhancement saturation effects due to L_{eff} and laser power for highly enriched 100 Modern sample and favorably changed the non-linearity between 12 Modern and 100 Modern samples. However, under the same operating conditions, the normalized OG signal for 1 Modern sample is higher than that of 12 Modern. This result was somewhat confusing and required analyzing samples with concentrations in between these values. Since we didn't have calibration samples with these values, we performed dilution experiments as follows: First, a 1.1 Torr of 100 Modern sample is trapped in the analysis cell and measured while the reservoir is being pumped down and filled with 1 Modern CO_2 gas. After recording the signal amplitude for 100 Modern, the cell is filled with 1 Modern CO_2 and pumped back down to 1.1 Torr and the dilution factors correspond to isotopic ratios given in Figure 5.5.
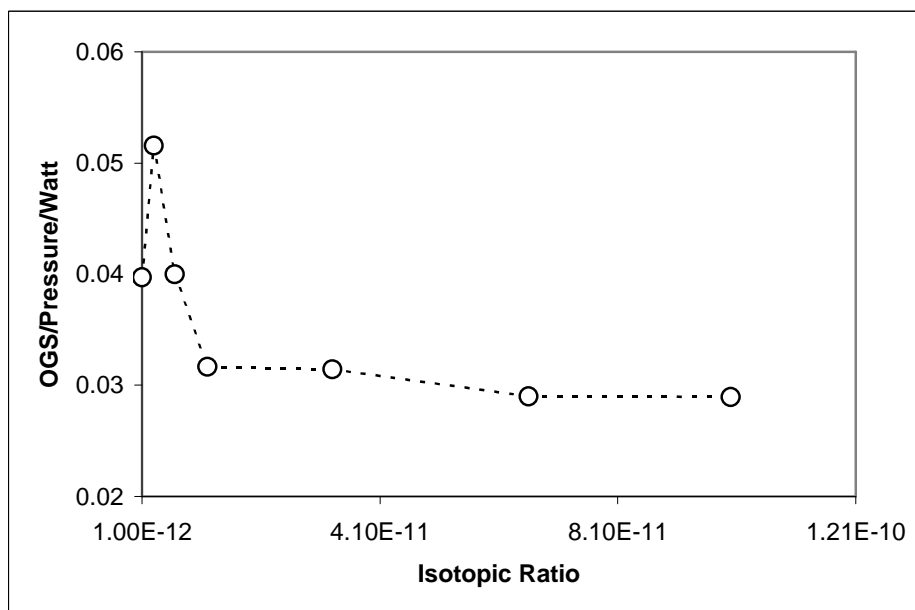
Figure 5.6 Calibration obtained by diluting 100 Modern CO_2 sample with 1 Modern CO_2.

It is apparent from the figure that the signal enhancement is higher around 1 Modern value, although the signal amplitudes are slightly different for those concentration values plotted in Figure 5. This probably is due to memory effect and/or the 12 Modern signal amplitude in Figure 5 has a larger uncertainty than estimated. One main difference between experimental procedures is that the cell is not heated and pumped down for extended period of time between measurements as it was done for the calibration plots in Figure 4.8 and 4.9.

As mentioned in chapter 4, calibration studies in flow mode operation also showed a decrease in signal enhancement for "high" radiocarbon concentrations (>1.5 Modern) at low laser modulation frequencies (17 Hz). However compared to batch mode measurement procedure, this effect is observed at a lower concentration, that is, when the

radiocarbon concentration is increased from 1.5 Modern to 12 Modern. In addition, signal

dependence on laser power behaved differently, as shown in Figure 5.7.
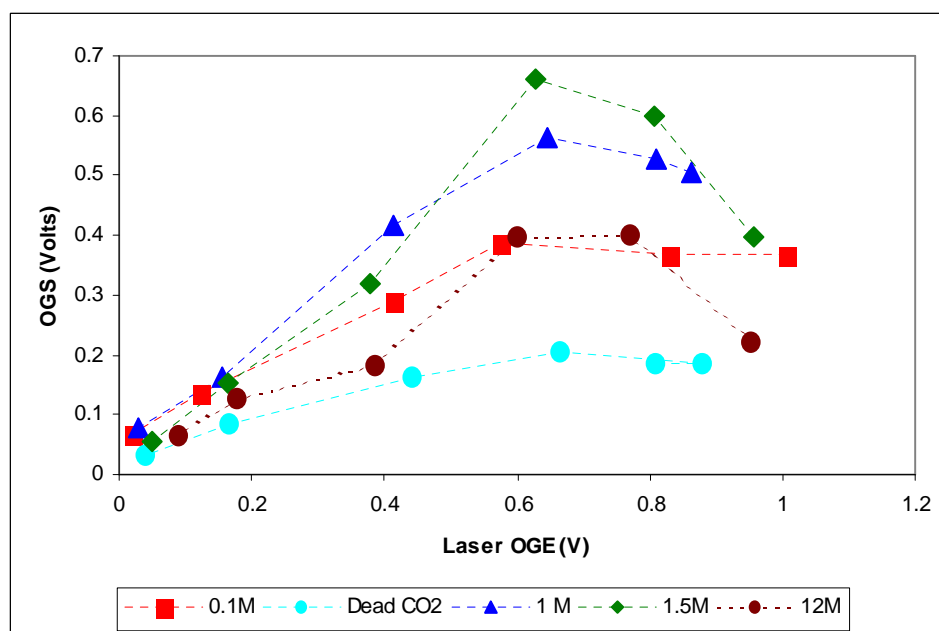
Figure 5.7 OG Signal show different laser power dynamics for different ^{14}C sample concentrations.

In this case, the x-axis values are the optogalvanic signal output from the laser's power

supply, which has a linear relationship with the actual laser output power as shown in

Figure 5.8.
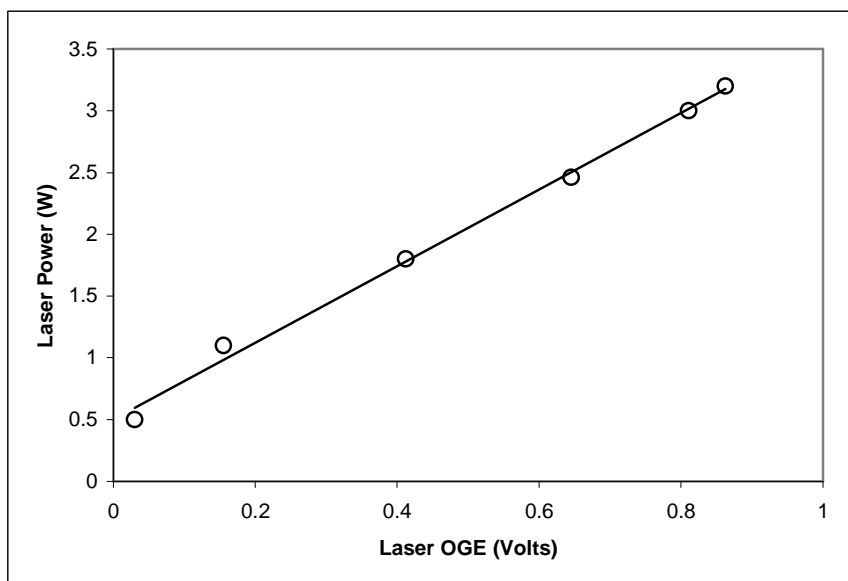
Figure 5.8 The optogalvanic signal obtained from the power supply is proportional to laser power

Figure 5.7 shows the OG signal variation for increasing laser intensity for the concentrations that correspond to the calibration points indicated in Figure 4.11. Figure 5.7 also includes the data for the 12 Modern sample which was mentioned in the text. The optogalvanic signal due to the background behaves differently than that of resonant $^{14}CO_2$ signals. Background signals clearly show saturation effects with laser power increase. However, for the resonant $^{14}CO_2$ signals, we observe a decrease in signal beyond ~2 Watt laser power and this effect is bigger as the radiocarbon amount is increased. For the case of batch mode measurements (Figure 5.4) we did not observe such behavior except for the highest enrichment of 100 Modern. At higher laser modulation frequencies, it was observed that this effect occurred at higher laser power values, as indicated in Figure 5.9 below.
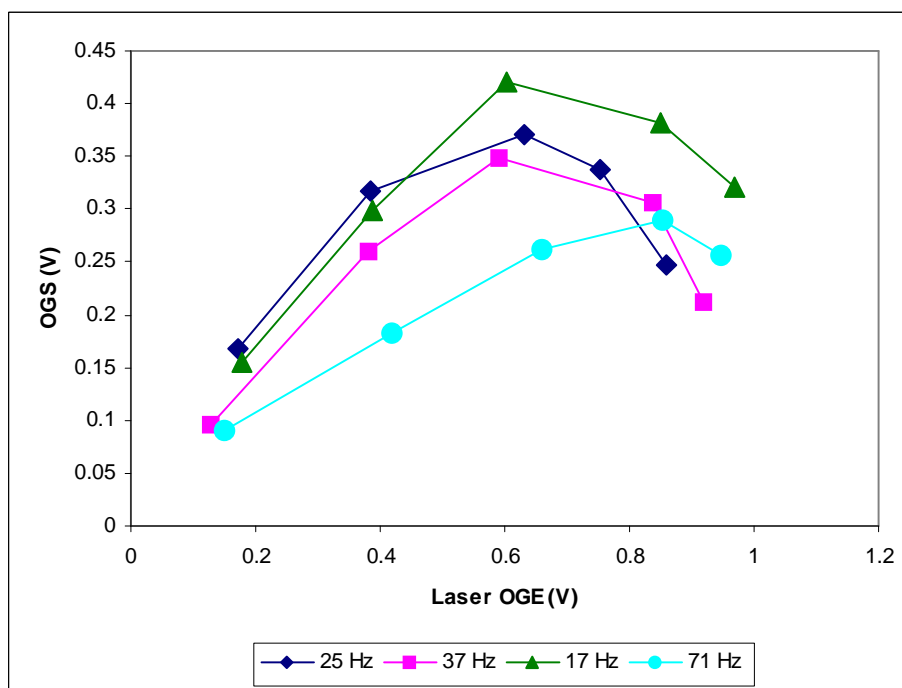
Figure 5.9 Laser power and OG signal relation at different laser chopping frequencies. The sample is 1 Modern pure CO_2 flowing at 0.05 sccm

As seen from the figure above, the linearity is different at higher modulation frequencies. At shorter measurement times, i.e. higher chopping frequencies, the optogalvanic signal, and thus the signal enhancement decreases non-linearly at higher laser intensities. Therefore, analogous to the batch mode measurement procedure, shorter measurement times and lower laser powers is favorable for obtaining a larger calibration interval.

In Figure 4.12, it was indicated that the optogalvanic signal increases with increasing flow rate. Under the given discharge conditions with sample being pure CO_2 the resonant laser interaction causes local heating of the gas due to absorption. Fresh gas flowing into the analysis cell which is cooler than the discharge increases the temperature gradient and therefore the variation in the particle number density which we observe as an increase in

the optogalvanic response. Those experiments were carried out with pure CO_2 gas with 1 Modern ^{14}C and the laser power was set around 0.6 V of Laser OGE indicated in Figure 5.7 above. Therefore it is now believed that the decrease in ^{14}C OG signal in Figure 5.7 for values greater than ~ 2 Watt of laser output power is due to the change in gain conditions of the discharge. It is clear that the OG signal is enhanced for the background indicated by the "dead CO_2" but it shows saturation with increased laser power. However when the cell contains resonant $^{14}CO_2$ molecules, optogalvanic signal changes sign beyond this threshold value and causes the observed decrease in the signal amplitude. That is, the gain conditions are different for the background and the resonant ^{14}C molecules.

5.3   Theoretical Model

The results presented so far clearly indicate the huge enhancement in signal sensitivity via intracavity technique depend on several factors including laser power, laser modulation frequency, flow rate and the $^{14}CO_2$ laser operating at a wavelength close to end of its cavity mode. A comprehensive model of the optogalvanic signal generation inside the laser cavity requires quantitative analysis of rate equations that describe the variations of these parameters with time. Atmanspacher et al [72] have studied the related dynamics of Intracavity Absorption Spectroscopy with a multimode laser by numerical analysis of a set of rate equations for the laser medium, the absorbing medium and the number of cavity photons which provide the coupling between the laser gain medium and the absorber. For the case of a single mode laser like ours, the equations for the laser gain medium, can be written as:

$$\frac{dn_{inv}}{dt} = p - A_{inv}n_{inv} - B_{inv}n_{inv}E_{photon}N_{photon} \tag{1}$$

Here p is the pumping rate, A_{inv} is the Einstein A coefficient of the upper laser level, n_{inv} is the number of upper level molecules, N_{photon} is the number of photons, E_{photon} is the energy of an emitted photon and B_{inv} is the Einstein B coefficient of the inverted state. The rate equation for the resonant population densities of the intracavity absorbing (or gain) medium is given by,

$$\frac{dn_2}{dt} = -\frac{dn_1}{dt} = B_{12}(n_1 - n_2)E_{abs}N_{photon} - A_{21}n_2 \tag{2}$$

where E_{abs} is the energy of the absorbed photons, n_1 and n_2 are the population densities in the lower and upper levels, respectively, A_{21} is the Einstein A coefficient of the upper level and B_{12} is the Einstein B coefficient for the absorbing transition.

The coupling between the laser gain medium and the intracavity medium is described by the rate equation for the change in number of photons, as follows:

$$\frac{dN_{photon}}{dt} = B_{inv}n_{inv}E_{photon}(N_{photon} + 1) - \left(\frac{N_{photon}}{T_{photon}}\right) - B_{12}(n_1 - n_2)E_{abs}N_{photon}$$

$$- B'_{12}(n'_1 - n'_2)E_{abs}N_{photon} \tag{3}$$

The first part is the stimulated emission term due to the laser gain medium and the second term represents the broadband cavity losses where the photon lifetime T_{photon} is given by $T_{photon} = \dfrac{L}{c\sigma}$ and L is the cavity length and σ represents the losses per cavity round trip due to the laser output, diffraction, scattering, etc. The last two terms comes from equation (2) for the resonant population densities without the contribution of the spontaneous emission term and including a non-resonant background contribution. The

populations of background molecules in the lower and upper levels are indicated by n'_1

and n'_2.

The ICAS technique is based on measuring the emission spectrum of a laser in the presence of an intracavity absorber and variations in laser output are characterized by Eq (3). However, ICOGS only measures the electrical signal which arises due to resonant and non resonant laser interactions altering equilibrium population distributions in the intracavity cell and it is related to the last two terms in Eq. (3). The number of resonant molecules in the analysis cell ($\sim 3.55 \times 10^4 / cm^3$) is negligible compared to the active molecules in the laser medium ($\sim 7.0 \times 10^{16} / cm^3$). For the 50 W internal laser power, it is estimated that only $\sim 5 \times 10^{-13}$ % of the cavity photons would be resonantly absorbed in the internal cell, which will have no measurable effect on the laser output. In addition, even though for the non-resonant term the population difference can be large due to natural abundance, at the $^{14}CO_2$ line center, the line strength is reduced by more than 10 orders of magnitude and $B_{12} >> B'_{12}$.

According to temperature model of the optogalvanic effect, as explained in Chapter 2, the OG signal arises as a result of change in molecule number density in the irradiated part of the discharge that leads to a change in its electrical properties. When the system is considered to be in absorptive mode, energy is gained from the incoming radiation due absorption, the rate of which is given by:

$$\frac{dE_1}{dt} = \sigma_{12} I_{12} \Delta n$$

where σ is the absorption cross section, I is the laser intensity and Δn corresponds to population difference between the upper and lower laser levels. In general, dynamic behavior of level populations is given by the relation: [77]

$$\frac{d(\Delta n_i)}{dt} = \sum_j \gamma_{ji} \Delta n_i - \sum_j (n_i - n_j) \sigma_{ij} I_{ij}$$

where γ_{ji} are the rate constants for transitions without the laser perturbation. In the case where the OG effect reaches an equilibrium, $d(\Delta n)/dt = 0$ If we label the lower laser level as 1,

$$\Delta n_1 = -(n_1 - n_2) \sigma_{12} I_{12} T_1$$

and

$$\Delta n_2 = (n_1 - n_2) \sigma_{12} I_{12} T_2$$

where T_1 and T_2 characterize the relaxation time to reach steady state after laser irradiation. Another advantage of ICOGS over ICAS is the fact that the sample is kept in a glow discharge that maintains excited state populations of molecules which are not populated under normal conditions. Therefore in addition to laser pumping term, the net rate equation for the upper laser level must contain collisional energy exchange term with Nitrogen, collisional exchange terms due to electron impact excitation and also the *V-V-T* de-excitation (see Chapter 2), which may all effect T_1 and therefore the OG signal. Overall temporal behavior of the system can be described by constructing the rate equations for all the relevant vibrational levels including the energy exchange rates between them.

In addition to OG signal increase with laser intensity and measurement time, the results of the experiments with 100% CO_2 indicated that the highest enhancement in signal sensitivity was obtained at a specific detuning point from the line center of the laser's spectral gain profile, as shown in Figure 4.10. As the laser is tuned across its gain profile, the decrease in the laser gain is compensated by increased gain in the analysis cell without causing any change in the laser output power [28]. However as illustrated in Figure 4.6, numerical analysis by Baev et al showed with ICAS using a single mode laser, a maximum value of sensitivity enhancement of ~10^7 can be achieved compared to an external cell measurement only when the laser operates close to its lasing threshold. But also as mentioned in the text, it is impossible to achieve this enhancement in practice with absorption spectroscopy due to the requirement of laser power detectors that is sensitive enough to detect variations of as low as 10nW. With the calibration intervals presented in Chapter 4, we have shown that similar signal enhancement is possible when optogalvanic spectroscopy technique is utilized. The maximum enhancement is at the point of spatial mode hopping but not laser threshold. At that point, the laser is operating at ~ 4 times higher than its threshold power.

A comprehensive numerical model for the optogalvanic signal enhancement inside a laser cavity requires detailed numerical analysis of rate equations that include all the variables mentioned above and is left for future work.

5.4　Effects of Nitrogen as a Carrier Gas on OG Signal Enhancement

In Chapter 2, it was mentioned that the having Nitrogen in the analysis cell, enhanced the OG signal for the same reason a CO_2 laser output is increased by efficient energy transfer

between electronically excited nitrogen molecules and upper laser level of CO_2. Highest SNR values in previous external cell measurements for stable isotope ratio analysis of CO_2 were obtained around 5% CO_2 in Nitrogen. Therefore, initial experiments of ICOGS were carried out with Nitrogen as the buffer gas. This way, we demonstrated that it is possible to perform rapid analysis by sample injection onto a non-resonant carrier gas while using a lot less CO_2 sample compared to pure CO_2 measurements. Figure 5.11 shows a typical experiment carried out with this method, where 0.5 ml of 100 Modern CO_2 is injected onto a stream of nitrogen gas while the cell pressure is kept constant at 5 Torr. That is the cell contains only 0.25 micrograms of CO_2 at the peak of the curve.
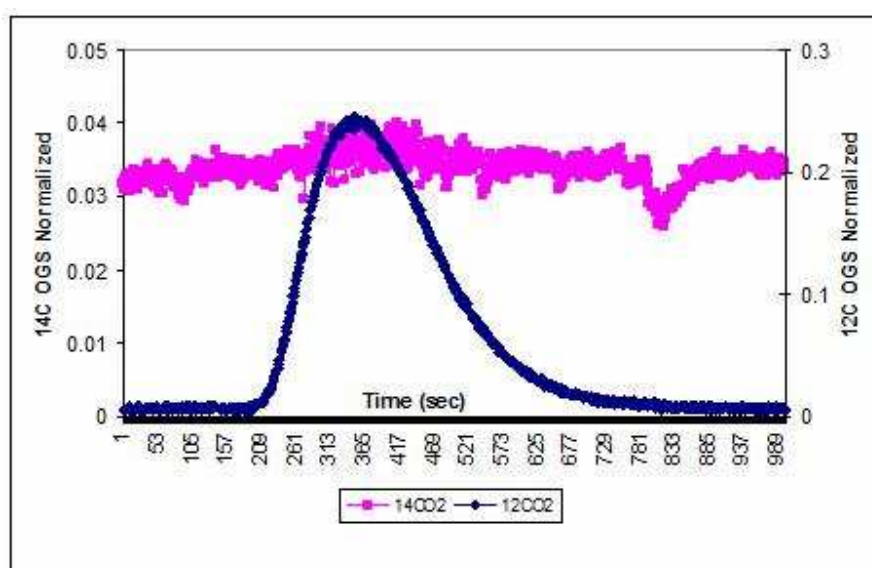
Figure 5.10 An axample run in the flow mode. 100 Modern pure CO_2 sample injected onto a stream of Nitrogen gas.

In the flow mode experiments where N_2 is used as a carrier gas, the $^{12}CO_2$ is measured in external cavity configuration. The OG signal obtained with this laser clearly shows the increase and decrease in the CO_2 content of the gas. However, ICOGS signal increase and decrease due to $^{14}CO_2$ laser interaction is relatively small. This is likely to be due to the

fact that having the analysis cell inside the laser cavity together with Nitrogen carrier, gain per molecule is so high that we are sensitive to only trace amounts of residual radiocarbon and as the enrichment is increased, system is approaching to a level of gain saturation.

Using different higher enrichments, a calibration curve could be obtained using nitrogen as carrier gas as shown in Figure 5.12 below.
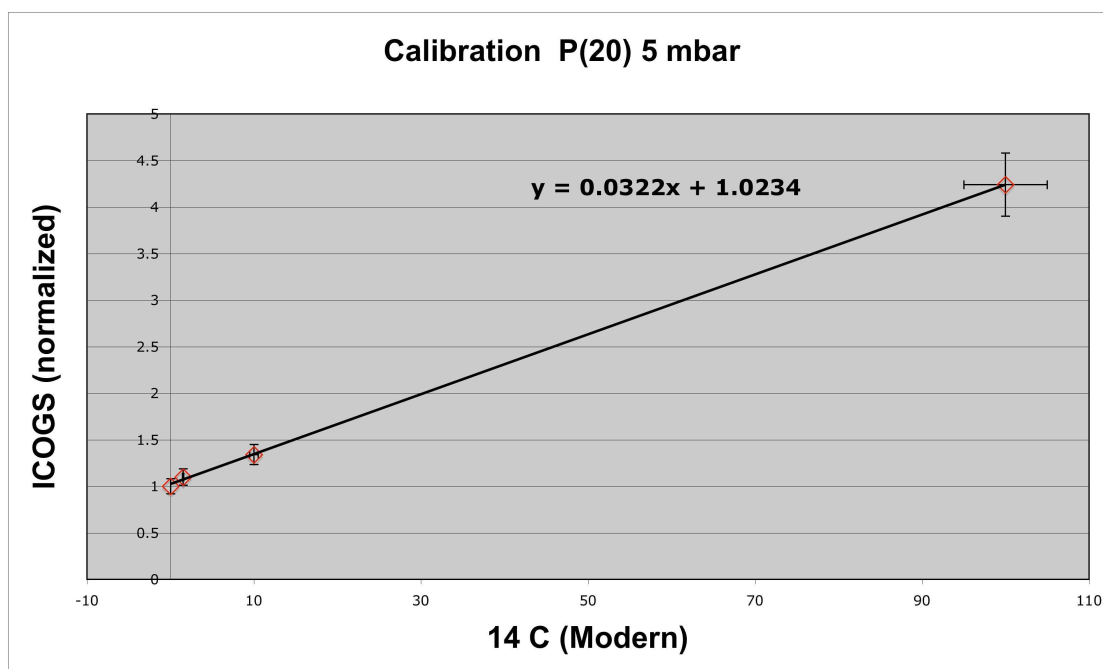
Figure 5.12 Calibration curve obtained using nitrogen as a carrier gas.

The slope of the curve implies that the OG signal grows only 3% for every modern increase. Therefore, in order to get more accurate results especially for unknown samples, the precision of the system has to be improved from the current conditions. In addition, these data were obtained at 5 mbar with long measurement time (low chopping

frequency) and high laser power. More work remains to be done to determine the optimum conditions for calibration using Nitrogen as carrier gas.

5.5   Summary

The results presented show that the signal enhancement with this new method enabled us to measure trace amounts of radiocarbon. However the system is very non-linear when the resonant molecule concentration changes over several orders of magnitude. The dynamic range of the calibration depends on several factors. Therefore the general equation for optogalvanic signal given in Eq 2.8 is linear only for small variations in several interrelated parameters which are summarized in Figure 5.14, below. The calibration results indicate that signal enhancement over conventional external cell measurement, given by the effective path length is of the order of 10^6 and it is proportional to measurement time up to 25 msec.
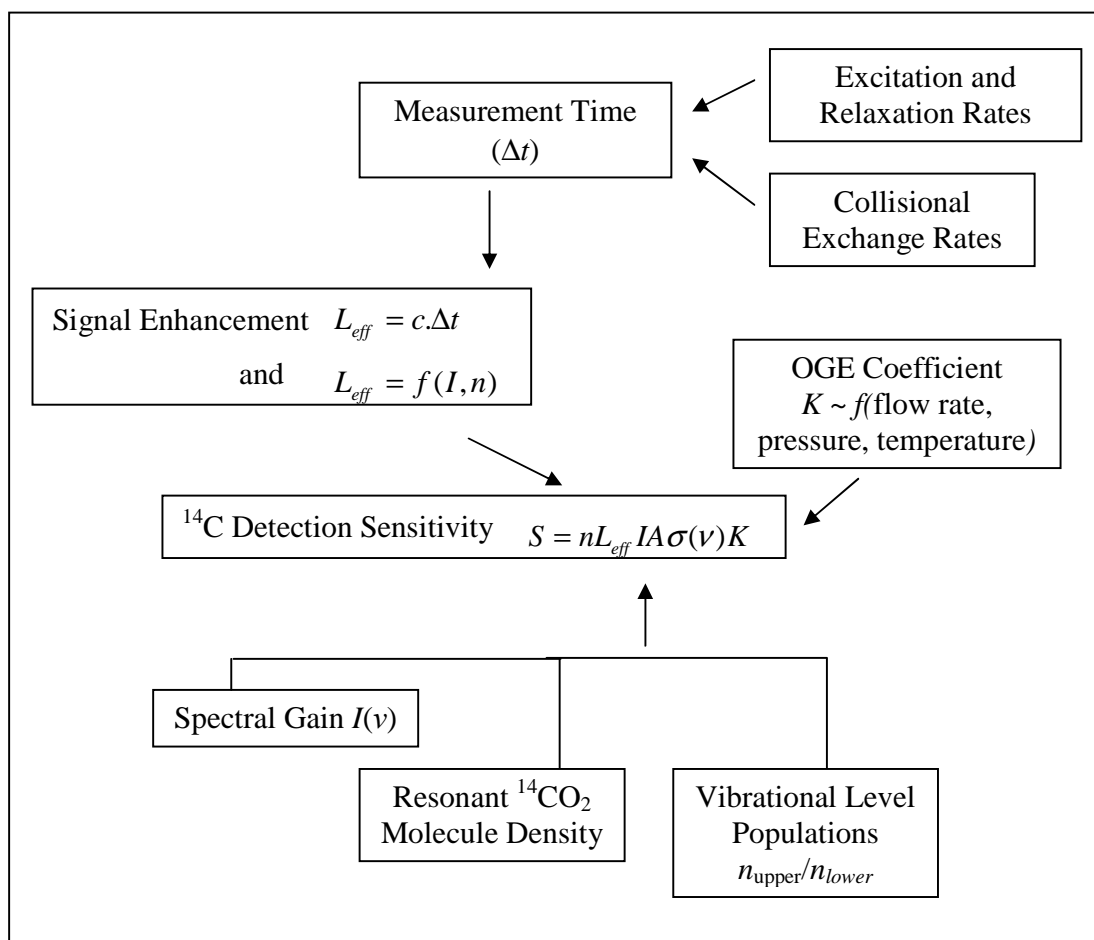
Figure 5.14 Summary of different paramaters that determine the sensitivity of ICOGS. Sensitivity is different for signal and the background.

Laser chopping frequency also effects the OG equilibration time and hence the signal amplitude. The dynamic range of the calibration intervals depend on the signal enhancement which can be controlled by varying measurement time and laser intensity. More abundant isotope contribution can be reduced by adjusting the gas pressure. Also

by controlling the flow rate, gas temperature can be varied to obtain enhanced optogalvanic response.

Chapter 6 :   Conclusions

6.1   Summary

The calibration intervals and experimental observations presented in the preceding chapters show that we have successfully developed a laser based radiocarbon analyzer that can compete with state of the art Accelerator Mass Spectrometer in various fields of applications, including biological sciences, environmental CO_2 monitoring and carbon dating. With this technique, it will be possible to quantify of ^{14}C-labeled sub-microgram bio-molecules having enrichments around 1 to several hundred Modern more rapidly in a lab setting with less complexity and more cost effectively than with AMS. In addition, continuous carbon isotope ratio monitoring using flow through measurement capabilities of ICOGS with precision around 1δ will improve our understanding of regional carbon budgets and human influence on the climate change. The measurement sensitivity and limit of detection achieved with this new technique enable us to determine radiocarbon age of a wide variety of samples.

The technique is based on laser optogalvanic effect and the huge enhancement in signal sensitivity over the conventional single or multi pass external cell configuration is achieved by placing the analysis cell inside a laser cavity. This new approach is analogous to well known Intracavity Absorption Spectroscopy (ICAS) method with major differences. Firstly, the detection is electrical rather than optical. That is even though the cavity loss or additional gain introduced by the intracavity sample cell does not have a measurable effect on the laser emission, impedance variations from the equilibrium conditions of the glow discharge can be measured with high SNR. Secondly,

different from ICAS with single mode lasers, we have achieved highest enhancement by making use of a single mode laser. The contents of the analysis cell is similar to that of the laser medium and the as the laser is tuned away from it's line center, the losses are compensated by the additional gain in the cell which manifest itself as enhancement in the signal sensitivity. The enhancement achieved is characterized by an effective path length increase given by $L_{\text{eff}} = c.\Delta t$, where Δt is related to the measurement time. The enhancement is different for the resonant signal and the non-resonant background, as explained in Chapters 4 and 5. We have shown calibration curves that cover a dynamic range from "dead" CO_2 ($< 10^{-3}$ Modern) to 100 Modern. For extended dynamic ranges, laser power and measurement time need to be varied to control the effects of enhancement saturation, as described in Chapter 5. A summary of the different parameters that effect the sensitivity and signal enhancement of this new method is given in Table 5.14.

6.2   Future Work

Continued work on this new analytical measurement technique can be divided into two main topics. First, a comprehensive numerical analysis of the governing rate equation system which will perfect our understanding of the signal enhancement mechanisms needs to be completed. Second, further experimental work can be done to improve the precision of the instrument as well as its accuracy in the high frequency regime. In his thesis work, Okil [43] has demonstrated a precision of 0.1δ in his external cell measurement system. This was mainly achieved by measuring the double ratio of the

sample cell with a reference cell as explained in Chapter 2, above. Therefore, an external reference cell with enriched $^{14}CO_2$ will help improve the precision of ICOGS by at least an order of magnitude from its current value of ~ 3-4%. The accuracy of the instrument especially for the high frequency experiments will be improved by instrument engineering, in particular, by data acquisition software with a better phase locking algorithm. New software should also include coherent waveform analysis algorithm which is based on measuring the area under the OG waveform, as opposed to using only the signal at the fundamental frequency. Using this method, Okil [43] has demonstrated about 20% improvement in SNR.

Another experimental improvement on the performance of ICOGS must include developing better sample handling procedures. This new instrument can be coupled with other commercially available GC/LC instruments which will increase sample throughput and also make it possible to oxidize carbon containing compounds to CO_2 samples in situ. Collaborations with expert groups in the aforementioned applications fields will also be useful in technology transfer of the ICOGS system to the wider scientific community.

References

[1]   F.N.D. Kurie, A New Mode of Disintegration Induced by Neutrons, Phys. Rev., **45** 904 (1934)

[2]   S.A. Korff and W.E. Danforth, Neutron Measurements with Boron-Trifluoride Counters, Phys. Rev., **55** 980 (1939)

[3]   H.A. Bethe and S.A. Korff and G. Placzek, On the Interpretation of Neutron Measurements in Cosmic Radiation, Phys. Rev., **57** 573 (1940)

[4]   S. Ruben and M.D. Kamen, Long-Lived Radioactive Carbon: C^{14}, Phys. Rev., **59** 349 (1941)

[5]   W.F. Libby, Atmospheric Helium Three and Radiocarbon from Cosmic Radiation, Phys. Rev., **69** 671 (1946)

[6]   E.C. Anderson, W.F. Libby, S. Weinhouse, A.F. Reid, A.D. Kirshenbaum and A.V. Grosse, Natural Radiocarbon from Cosmic Radiation, Phys. Rev. **72** 931 (1947)

[7]   H.E. Suess, Radiocarbon Concentration in Modern Wood, Science **122** 415 (1955)

[8]   S. Solomon, D. Qin, M. Manning, Z. Chen, M. Marquis, K.B. Averyt, M. Tignor, H.L. Miller (eds) IPCC, 2007: Climate Change 2007: The Physical Science Basis. Contribution of Working Group I to the Fourth Assessment Report of the Intergovernmental Panel on Climate Change Cambridge University Press, Cambridge, United Kingdom and New York, NY, USA (2007)

[9]   NCRP Report 81, Carbon-14 in the Environment (1985)

[10]   I. Levin, Radiocarbon – A Unique Tracer of Global Carbon Cycle Dynamics, Radiocarbon, Vol: 42 No:1 69 (2000)

[11]   T, Naegler, Closing the global radiocarbon budget 1945-2005, Journal of Geophysical Research-Atmospheres, **111** D12311 (2006)

[12]   Q. Hua and M. Barbetti, Review of tropospheric bomb C-14 data for carbon cycle modeling and age calibration purposes, Radiocarbon Vol: 46 No: 3 1273 (2004)

[13]   G. Lappin and R.C. Garner, Big physics, small doses: the use of AMS and PET in human microdosing of development drugs, Nature Rev. Drug Discov. **2** 233 (2003)

[14]   H.A. Polach, Four Decades of LS Counting and spectrometry, Radiocarbon after four Decades. An interdisciplinary Perspective, R.E. Taylor, A. Long and R. Kra (eds) Springer-Verlag, NY (2003)

[15]   R.C. Garner et al, A validation study comparing accelerator MS and liquid scintillation counting for analysis of 14C-labelled drugs in plasma, urine and faecal extracts, Journal of Pharmaceutical and Biomedical Analysis **24** 197 (2000)

[16]   M. Salehpour, G. Possnert and H. Bryhni, Subattomole Sensitivity in Biological Accelerator Mass Spectrometry, Anal. Chem. **80**, 3515 (2008)

[17]   J. Vogel, K.W. Turteltaub, R. Finkel and D.E. Nelson, AMS Isotope Quantification at Attomole Sensitivity, Anal. Chem. **67** 353A (1995)

[18]   M. Balter, Radiocarbon Dating's Final Frontier, Science News Focus, **313** 1560 (2006)

[19]   D.E. Murnick, O. Dogru, and E. Ilkmen, Intracavity Optogalvanic Spectroscopy. An Analytical Technique for 14C Analysis with Subattomole Sensitivity, Anal. Chem. **80** 4920 (2008)

[20]   D.E. Murnick and B.J. Peer, Laser-Based Analysis of Carbon Isotope Ratios, Science **263** 945 (1994)

[21]   F. Parente and G. B. Porro, The ^{13}C-urea breath test for non-invasive diagnosis of Helicobacter pylori infection: which procedure and which measuring equipment?, European Journal of Gastroenterology & Hepatology. Vol:13 Issue:7 803 (2001)

[22]   J. Sierks, T. Latz, V.M. Baev, P.E. Toschek: Proceedings of the 1996 European Quantum Electronics Conference (EQEC'96), 8–13 September 1996, Hamburg, p. 100, QWB6

[23]   E. Kerstel and L. Gianfrani, Advances in Laser-based Isotope Ratio Measurements: Selected Applications, Appl. Phys B Vol: 92 Issue: 3 439 (2008)

[24]   E.R.T Kerstel, In: Handbook of Stable Isotope Analytical Techniques, ed. By P.A. de Groot (Elsevier, Amsterdam, 2004) Chapt. 34, 759

[25]   W. Demtröder, Laser Spectroscopy: Basic Concepts and Instrumentation, 2nd ed. Springer, Berlin (1996)

[26]   G. Berden, R. Peeters and G. Meijer, Cavity Ring-Down Spectroscopy: Experimental Schemes and Applications, Int. Reviews in Physical Chemistry, Vol. 19, No. 4, 565 (2000)

[27]   B.A. Paldus and A.A. Kachanov, An Historical Overview of Cavity Enhanced

Methods, Can. J. Phys. **83** 975 (2005)

[28] V.M. Baev, T. Latz, P.E. Toschek, Laser Intracavity Absorption Spectroscopy, Appl. Phys. B **69** 171 (1999)

[29] V. S. Burakov and S. N. Raikov, Intracavity Laser Spectroscopy: Plasma Diagnostics and Spectral Analysis (Review), Journal of Applied Spectroscopy, **69** No. 4 (2002)

[30] T. Matsushima, J. Kawanabe, H. Maekawa, S. Saimi, T. Suetat, and Y. Chott, High Sensitivity Isotope Concentration-Ratio Measurement CO_2 Infrared Laser System (II), 25th International Conference on Infrared and Millimeter Waves, Conference Digest, 151 (2000)

[31] B. Barbieri, N. Beverini, A. Sasso, Optogalvanic Spectroscopy, Rev. Mod. Phys. **62** 603 (1990)

[31] P.D. Foote, F.L. Mohler, Photo-Electric Ionization of Caesium Vapor, Phys. Rev. **26** 195 (1925)

[32] A. Garscadden, P. Bletzinger and E.M. Friar, Moving Striations in a He-Ne Laser J. Appl. Phy. **35** 3432 (1964)

[33] M.L. Skolnick, Use of Plasma Tube Impedance Variations to Frequency Stabilize a CO_2 Laser, IEEE J. Quant. Electron. **QE-6** 139 (1970)

[34] C.-C. Tsai, T. Lin, C. Shieh, T.-C. Yen, and J.-T. Shy, CO2 laser frequency stabilization using the radio-frequency optogalvanic Lamb-dip Appl. Opt., Vol. 30, No. 27, (1991)

[35] R.B. Green, R.A. Keller, G.G. Luther, P.K. Schenck and J.C. Travis, Galvanic Detection of Optical Absorptions in a Gas Discharge, Appl. Phys. Lett. **29** 727 (1976)

[36] G. C. Turk, W. G. Mallard, P. K. Schenck, and K.C. Smyth, Improved sensitivity for laser enhanced ionization spectrometry in flames by stepwise excitation, Anal. Chem., **51** 2408 (1979)

[37] J. C. Travis, G. C. Turk, and R. G. Green, Laser-enhanced ionization spectrometry, Anal. Chem., Vol.54 Iss:9 1006A (1982)

[38] M.N. Reddy, Laser Optogalvanic Spectroscopy: Experimental Details and Potential Applications in R&D, Defense Science Journal, Vol 44, No 4 279 (1994)

[39] P. Pianarosa, Y. Demers, and J. M. Gagne, Isotopic analysis by optogalvanic spectroscopy, J. Opt. Soc. Am. B Vol. 1, No. 5 704 (1984)

[40] C. K. Patel, Selective Excitation Through Vibrational Energy Transfer and Optical Maser Action in N_2-CO_2, Phys. Rev. Lett. **13** 617 (1964)

[41] D. E. Murnick, M. J. Colgan, H. P. Lie and D. Stoneback, Stable Isotope Analysis of Breath Using the Optogalvanic Effect, SPIE Bios '96 Proceedings, **2678**, 454 (1996)

[42] V. Savarino, Md, F. Landi, Md, P. Dulbecco, Md, C. Ricci, Md, L. Tessieri, Md, R. Biagini, Md, L. Gatta, Md, M. Miglioli, Md, G. Celle, Md, and D. Vaira, Md, Isotope Ratio Mass Spectrometry (IRMS) Versus Laser-Assisted Ratio Analyzer (LARA), Digestive Diseases and Sciences, Vol. 45, No. 11 2168 (2000)

[43] J.O. Okil, PhD Thesis, Rutgers, The State University of New Jersey, Newark, NJ (2004)

[44] Y. P. Raizer, M.N. Shneider, N.A. Yatsenko, Radio-Frequency Capacitive Discharges, CRC Press (1995)

[45] K. Marcus and J. A. C. Broekaert, Glow Discharge Plasmas in Analytical Spectroscopy, John Wiley and Sons (2003)

[46] J.E.M. Goldsmith and J.E. Lawler, Optogalvanic Spectroscopy, Contemp. Phys. Vol:22 No:2 235 (1981)

[47] S. Moffatt and A.L.S. Smith, Temperature Perturbation Model of the Opto-Galvanic Effect in CO2 Laser Discharges, J. Phys. D: Appl. Phys., **17** 59 (1984)

[48] W.W. Duley CO_2 Laser: Effects and Applications. New York: Academic Press (1976)

[49] C. Freed, L.C. Bradley and R.G. O'Donnell, Absolute Frequencies of Lasing Transitions in Seven CO2 Isotopic Species, IEEE Journal of Quantum Electronics, Vol: QE-16, No. 11 (1980)

[50] T. Aoki, C. Yamada and M. Katayama, Change of Discharge Current in CO_2 Plasma Induced by Q-switched CO_2 laser, Japanese Journal of Applied Physics, Vol: 10, No: 3 332 (1971)

[51] F.O. Shimizu, K. Sasaki and K. Ueda, Optogalvanic Effect Study of Vibrational Relaxation in CO_2 Laser Processes, Japanese Journal of Applied Physics Vol: 22 No: 7 1144 (1983)

[52] M. Tachikawa, H. Murakami, F. O. Shimizu and T. Shimizu, Novel Aspects of the Optogalvanic Effect in the CO_2 Laser Medium, Japanese Journal of Applied Physics **29** 958 (1990)

[53] Y. P. Raizer, M.N. Shneider, N.A. Yatsenko, Radio-Frequency Capacitive Discharges, CRC Press (1995)

[54] Svelto, O. Principles of Lasers. 4th Ed. Springer, New York. 1998.

[55] W.L. Nighan, Electron Energy Distributions and Collision Rates in Electrically Excited N_2, CO, and CO_2, Physical Review A, Vol. 2, No.5, 1989 (1970).

[56] C.K.N. Patel, Interpretation of CO_2 Optical Maser Experiments, Physical Review Letters, Vol:12, No:21 588 (1964)

[57] H. Statz, C.L. Tang, G.F. Koster, Transition Probabilities between Laser States in Carbon Dioxide, J. Appl. Phys. **37** 4278 (1966)

[58] C. Freed, CO2 Isotope Lasers and Their Applications in Tunable Laser Spectroscopy, Tunable Lasers Handbook, edited by F. Duarte, Academic Press (1995)

[59] G. McMahon, Analytical Instrumentation A Guide to Laboratory, Portable and Miniaturized Instruments, Wiley, England (2007)

[60] F.G. Kitson, B.S. Larsen, C.N. McEwen, Gas Chromatography and Mass Spectrometry, A Practical Guide, Academic Press, Florida (1996)

[61] T. J. Ognibene, G. Bench and J. S. Vogel, A High-Throughput Method for the Conversion of CO2 Obtained from Biochemical Samples to Graphite in Septa-Sealed Vials for Quantification of 14C via Accelerator Mass Spectrometry, Anal. Chem., **75** 2192 (2003)

[62] R.D. May and P.H. May, Solid State Radio Frequency Oscillator for Optogalvanic Spectroscopy: Detection of Nitric Oxide using the 2-0 Overtone Transition, Rev. Sci. Instrum., Vol: 57 No: 9 (1986)

[63] V. N. Ochkin, N.G. Preobrazhensky, N. Y. Shaparev, Optogalvanic Effect in Ionized Gas, CRC Press (1999)

[64] J.W. Choi, Y.B Chung, M. Strzelec and M. Kopica, Frequency Stabilization of a Radio Frequency Excited CO_2 Laser Using The Optogalvanic Effect, Review of Scientific Instruments, Vol: 69 No: 12 (1998)

[65] C. Tuniz, J.R. Bird, G.F. Herzog and D. Flink, Accelerator Mass Spectrometry: Ultrasensitive Analysis for Global Science, CRC Press, Boca Raton, Fla. (1998)

[66]   P.M. Milonni, J.H. Eberly, Lasers, John Wiley (1988)

[67]   W.T. Silfvast, Laser Fundamentals 2nd Ed, Cambridge University Press (2004)

[68]   T.W. Meyer, Charles K. Rhodes and H.A. Haus, High-Resolution Line Broadening And Collisional Studies In CO_2 Using Nonlinear Spectroscopic Techniques, Phys. Rev. A 12, 1993 (1975)

[69]   M.Abromowitz, I.A. Stegun, Handbook of Mathematical Functions with Formulas, Graphs, and Mathematical Tables, Courier Dover Publications, New York, (1965)

[70]   X. Huang, and Y.L. Yung, A Common Misunderstanding about the Voigt Line Profile, Journal of the Atmospheric Sciences, Vol. 61, Issue 13 (2004)

[71]   R.D. Van Zee and J.P. Looney (eds.) Cavity-Enhanced Spectroscopies, Experimental Methods in the Physical Sciences, Vol. 40, Academic Press, San Diego, CA (2002)

[72]   H. Atmanspacher, H. Scheingraber and C.R. Vidal, Dynamics of Laser Intracavity Absorption, Physical Review A, Vol. 32, No: 1, 254 (1985)

[73]   F. Trager, Springer Handbook of Lasers and Optics, Springer (2007)

[74]   H. J. Kimble, Calculated Enhancement for Intracavity Spectroscopy with a Single Mode Laser, IEEE Journal of Quantum Electronics, Vol: QE-16, No: 4 (1980)

[75]   S.J. Harris and A.M. Weiner, Continuous wave intracavity dye laser spectroscopy. II. A parametric study, J. Chem. Phys. 74, 3673 (1981)

[76]   A.L.S. Smith and M. Brooks, Radiation Field Induced perturbations in CO_2 laser plasmas: I. Current and Pressure Fluctuations. J. Phys. D: Appl. Phys. **12** 1237 (1979)

[77]   G. Erez, S. Lavi and E. Miron, A Simplified Theory of Optogalvanic Effect, IEEE J. Quant. Electron. QE-15 1328 (1979)

CURRICULUM VITAE

Erhan Ilkmen

1977	Born September 30 in Istanbul, Turkey
1995	Started undergraduate education in Department of Physics, Istanbul Technical University, Istanbul, Turkey
1998	Launched Pozitron, LLC, a startup company in the field of Automation and Computer Technology
2001-2003	Attended Rutgers University, Newark, NJ. Graduated with Honors with a BA in Physics and a minor in Mathematics
2003	Started Graduate Program in Applied Physics at Rutgers University, Newark, NJ
2005	Poster Presentation: "Sensitive Detection of ^{14}C using Laser Optogalvanic Spectroscopy", 22nd Meeting of the Northeast US Chapter of the International Isotope Society in Uncasville, Connecticut
2007	Article Published: "Laser based ^{14}C counting, an alternative to AMS in biological studies", D. E. Murnick, O. Dogru, E. Ilkmen, Nuclear Instruments and Methods in Physics Research Section B: Beam Interactions with Materials and Atoms, Proceedings of the Tenth International Conference on Accelerator Mass Spectrometry, Volume 259, Issue 1, Pages 786-789 (2007)
2007	Oral Presentation: "Intracavity Optogalvanic Spectroscopy", APS DAMOP Meeting, July 2007, Calgary, Alberta, Canada
2008	Article Published: "Intracavity Optogalvanic Spectroscopy: An Analytical Technique for ^{14}C Analysis with Subattomole Sensitivity", D. E. Murnick, O. Dogru, E. Ilkmen, Journal of Anal. Chem.; (Accelerated Article); 80(13); 4820-4824 (2008)
2009	Article in Press: "^{14}C Analysis at Attomole Sensitivity via Intracavity Optogalvanic Spectroscopy", Nuclear Instruments and Methods in Physics Research Section B: Beam Interactions with Materials and Atoms, Proceedings of the Eleventh International Conference on Accelerator Mass Spectrometry

2009   Article in Press: "High Sensitivity Laboratory Based ^{14}C Analysis for Drug Discovery", Journal of Labelled Compounds and Radiopharmaceuticals

2009   Ph.D. Applied Physics, "Intracavity Optogalvanic Spectroscopy for Radiocarbon Analysis with Attomole Sensitivity", Rutgers University, Newark, NJ